sustainability

MDPI

Article

Water Permeability of Kemafil Georopes with a Geotextile Core Made of Wool Waste Based on Laboratory and Field Tests

Andrzej Gruchot [1,*], Tymoteusz Zydroń [1], Mariusz Cholewa [1] and Jacek Stanisz [2]

[1] Department of Hydraulic Engineering and Geotechnics, University of Agriculture in Kraków, Mickiewicza 24/28, 30-059 Kraków, Poland; tymoteusz.zydron@urk.edu.pl (T.Z.); mariusz.cholewa@urk.edu.pl (M.C.)
[2] Mineral and Energy Economy Research Institute, Polish Academy of Science, Józefa Wybickiego 7 A, 31-261 Kraków, Poland; jstanisz@min-pan.krakow.pl
* Correspondence: andrzej.gruchot@urk.edu.pl

Abstract: This paper presents the results of laboratory and field tests on the hydraulic properties of georopes produced using the Kemafil technology from sheep wool waste generated in the textile industry. The laboratory tests included the determination of the basic physical parameters and filtration properties of georopes, as well as tests of the physical properties and water permeability of the experimental training ground. As part of the field research, measurements of water infiltration through 1.0, 2.0 and 5.0 m long georopes embedded in the ground were carried out in nine monthly cycles. The conditions of water flow through the georopes were monitored on the basis of georope resistance measurements. Numerical calculations were also performed to determine the conditions of water flow through the georopes and the process of water infiltration from the georopes into the ground. The laboratory tests have shown that the water permeability of georopes is high and, based on the filtration criteria, they can act as a drainage material. The field measurements showed that the resistance of the georopes changed over time and depended on the amount of water supplied and the absorbency of the ground. The results of the numerical calculations were consistent with the results of the field measurements, at the same time indicating that some water infiltrated into the ground in the vicinity of the georopes, meaning that under the conditions that prevailed during the experiment, the georopes can act as infiltration drainage systems in the ground.

Keywords: geocord; Kemafil technology; permeability; resistance

Citation: Gruchot, A.; Zydroń, T.; Cholewa, M.; Stanisz, J. Water Permeability of Kemafil Georopes with a Geotextile Core Made of Wool Waste Based on Laboratory and Field Tests. *Sustainability* **2024**, *16*, 9403. https://doi.org/10.3390/su16219403

Academic Editor: Abdul-Sattar Nizami

Received: 6 August 2024
Revised: 7 October 2024
Accepted: 25 October 2024
Published: 29 October 2024

1. Introduction

Human life and economic activities are inextricably linked to the production of waste. The amount of waste, its diversity and its composition change and depend on the wealth and the technological level of the society in which it was generated. Each type of waste poses a threat to the natural environment and should therefore be disposed of or recovered. The management of waste generated as a result of human industrial and agricultural activities requires a number of activities to identify potential opportunities for their reuse in accordance with the principles of environmental protection. The Waste Act, which is in force in Poland [1], indicates the need to take measures to prevent the occurrence of waste and limit its spread in the environment. Waste management is a set of activities aimed at maximizing the recovery of secondary raw materials or energy from waste and reducing the amount of waste stored in the environment. Waste management should be largely based on the use of waste as a secondary raw material for engineering purposes or as an additive used to improve the properties of the starting material.

In earth construction, solutions based on the use of all types of reinforcement that improve the mechanical properties of low-bearing soils are becoming increasingly common [2–6]. Most often, dispersed reinforcement is used in the form of synthetic fibres of various lengths. An interesting solution is to use biodegradable fibres, e.g., wool, for such

reinforcement, thus improving the strength parameters of the soil to a satisfactory extent, or at least not worsening them. On the other hand, as a result of biodegradation processes, nitrogen compounds are released from the wool, which supports the development of vegetation and thus improves the surface stabilization of, e.g., slopes.

A significant problem in the case of earth constructions, especially road constructions, is the need to secure slopes of embankments and road excavations. The variability of meteorological conditions may cause the erosion of slopes and, consequently, problems with the exploitation of earthworks. Geosynthetics are most often used to reduce the surface erosion of soil and engineering structures, and their scope of application is so large that their selection does not cause any problems. Geosynthetics placed on a slope surface limit the penetration of solar radiation, eliminate sudden temperature changes and maintain relatively constant soil moisture content. As a result, they create a favourable microclimate for germinating grass seeds and protective plants [7,8].

Another problem related to the operation of earth construction facilities—road or hydrotechnical—is the proper drainage of embankments or excavations, which can be implemented in various ways. The use of geosynthetics in earth constructions can be profitable and allows their use as a substitute for mineral materials (geotextiles, geomembranes) or as reinforcing elements (geogrids). Geosynthetics placed horizontally between the fine-grained subsoil and the aggregate have a separating function, which prevents mixing, but they can also create a drainage system. When used for filtration, the geotextile serves as a filter preventing the unwanted migration of small particles and enabling adequate water flow. The main problem with geotextiles used for filtration applications is their ability to transmit and retain soil particles and prevent clogging [9]. Geotextiles that are used for drainage are subject to soil loads and pressures resulting from external loads, e.g., road traffic in road construction [10]. The deformation of geosynthetics due to external load may change the pore size of the geotextile, which is associated with a reduction in its ability to retain particles or a change in hydraulic conductivity [11–13]. The dynamic load of the geosynthetic may also cause the forced flow of fine soil particles [10]. Unfortunately, there is no universal solution in which a geotextile is compatible with all types of soil. Attempts are being made to develop design solutions in which geotextiles are adapted to certain types of soil, taking into account simple parameters resulting from particle size and density. It should be noted that the existing criteria related to water filtration through drainage materials may be insufficient when assessing the suitability of geosynthetics for filtration purposes [14,15].

There are a number of reports in the literature on the potential use of synthetic fibres for soil reinforcement. Synthetic fibres improve the properties of soils by increasing their tensile and compressive strength [16] as well as shear strength [17]. Studies on the use of natural fibres as replacements for synthetic fibres in soil composites have also been published in the literature [18–22]. From a sustainability point of view, natural fibres are replacing synthetic fibres for economic and ecological reasons. Natural fibres, in addition to their environmental advantages (high availability, low cost, renewability, biodegradability), have desirable mechanical properties (high strength-to-weight ratio, low density of 1.2 to 1.6 g cm^{-3}) and are generally able to guarantee the good mechanical properties of a composite, such as tensile strength, stiffness, flexural strength and flexural modulus [23]. The results of a study on the use of wool from the fleeces of domestic sheep ('Valle del Belice' from Sicily) to reinforce building elements of compacted soil are described, among others, in the work of Parlato et al. [24]. It should be clearly emphasized that the authors used natural fibres from agricultural waste from sheep with low-quality wool, which is not used in the textile industry and has to be landfilled. The addition of natural fibres to the mix of mineral-based building materials allowed them to improve tensile strength, toughness, impact resistance and durability and reduce shrinkage during drying. Sheep's wool is widely regarded as one of the most efficient insulating natural fibres due to its hygrometric and acoustic properties [25]. In the building sector, sheep wool meets the requirements for green building components, as it is an environmentally friendly material

found in excess, renewable annually and completely recyclable [26,27]. Composite materials have a wide range of properties and play an important role in environmental protection. The most common fibres used in composites are those obtained by chemical processes. However, natural fibres are increasingly being recognized as a potential component of biodegradable composites due to sustainability principles, environmental concerns and the fact that they are biodegradable. Biodegradable polymers are becoming an alternative to plastics, which have a negative impact on the environment [28]. In general, the skilful use of natural products including, for example, sheep's wool offers significant sustainability benefits, such as reduced production costs for new insulation materials and reduced environmental pollution.

The aim of this study was to assess the hydraulic properties of innovative, ecofriendly, biodegradable georopes produced from wool waste generated in the textile industry with Kemafil technology. Kemafil georopes have successfully been used for shallow reinforcement and the anti-erosion of slopes so far, but their hydraulic properties in field (real-world) conditions have not yet been tested. The research hypothesis was that the georopes, during their initial period of use, could act as a drainage system that disperses water into the surrounding soil, allowing the slope scarification process to accelerate.

2. State of the Art

The use of geosynthetics in earth-made structures for the regulation of water seepage requires various requirements to be fulfilled. In the case of granular materials used in the construction of filters, the most popular is the Terzaghi criterion [9], which proposes the criteria of retention (Equation (1)) and hydraulic conductivity (Equation (2)):

$$d_{15}^{f} \leq 5\, d_{85}^{S} \tag{1}$$

$$d_{15}^{f} \geq 5\, d_{15}^{S} \tag{2}$$

where dx is the grain size at x [%] passing, with the superscripts f and s denoting the filter and soil, respectively.

According to Giroud [29], possible overpressure resulting from too high of a hydraulic drop in accordance with Darcy's law and conservation of mass will not occur when:

$$k_s^{gr} \geq i_s\, k_s^{s} \tag{3}$$

where i_s is the hydraulic gradient in soil and k_s is the coefficient of permeability, with the superscripts gr and s denoting the granular filter and soil, respectively.

The design of a filter using geosynthetics is completely different. In this case, the selection of a geotextile includes its properties and the conditions of its operation in the ground, i.e., its retention properties, clogging and hydraulic conductivity [30]. The retention criterion is related to the pore diameter of the geotextile presented as O_{95} and is expressed by the equation:

$$O_{95} \leq \alpha\, d_{85}^{s} \tag{4}$$

where O_{95} is the filtration opening size of the geotextile and α is the retention ratio (representing the equivalent diameter of soil particles capable of penetrating the geotextile).

The assessment of the clogging rate of geotextiles can be performed using the long-term flow test [31] or tests recommended by American standards such as the hydraulic conductivity ratio test [9] or the Gradient Ratio (GR) test [9,14,15,32].

However, the criterion of hydraulic conductivity for geosynthetics states that:

$$k_s^{gt} \geq \gamma\, k_s^{s} \tag{5}$$

where γ is an empirical coefficient, the value of which ranges from 0.1 to even 1000 [9,33], and k_s is the coefficient of permeability, with the superscripts gt and s denoting the geotextile and soil, respectively.

In the case of geosynthetics, attention should also be paid to their thickness and internal stability [34]. The above analysis indicates quite significant discrepancies between the criteria applicable to assessing the suitability of earth materials to be used as filters and geosynthetics used for similar purposes.

Therefore, the use of georopes made using Kemafil technology from various materials requires knowledge of the filtration properties of all components. As a consequence, the adoption of individual criteria for the applicability of a given material may be insufficient and water permeability tests should also be carried out for Kemafil georopes made of specific materials. Research of this type is an important source of information on where and how Kemafil georopes can be applied.

One type of geosynthetics is geotextiles, which are used in civil engineering for separation, reinforcement, filtration, drainage, barriers and the protection of the ground. To protect slope surfaces, long-term protection geosynthetics can be used (3D mats, synthetic fibre nets, georopes), i.e., made of non-biodegradable, long-lasting materials that allow the use of their anti-erosion function for a period of at least a dozen or so years [35]. Temporary anti-erosion protection is carried out with biodegradable geosynthetics (mats and non-woven fabrics made of cotton, wool, jute or coconut fibres), which provide direct anti-erosion protection for up to 5 years. Materials of this type protect slopes against surface erosion in the early phase of development of the protected vegetation. Later, they decompose, providing nutrients for the development of vegetation, which ultimately takes over the function of anti-erosion protection [15,36,37]. Geosynthetics produced from biodegradable raw materials can be an alternative to traditional methods of surface slope protection, such as hydroseeding or turfing [38–40].

Natural fibres can be divided into three groups, depending on their origin—plant (cellulose), animal (protein) and mineral fibres [41]. Plant fibres are obtained from seeds, stems, leaves and fruits. Animal fibres are obtained mainly from wool and silk [42,43]. Mineral fibres, mainly asbestos, play a marginal role in environmental engineering. The mechanical, physical and chemical properties of fibres depend on their type and the processes to which they are subjected from the moment of collection to the final product. Obtaining specific types of fibres requires their collection, pushing, cleaning and drying. Although most natural fibres have high cellulose content, while animal fibres contain high amounts of protein, their structure and properties may be varied. These differences are reflected, among others, in the mechanical properties of a given material, as well as in the rate of the degradation process [43,44]. Regardless of their properties, fibres can be processed into threads, ropes, mats, textiles and nets. They can also be used as components of composite materials [45].

When water erodes the slope surfaces of soil embankments, this acts as the beginning of their destruction, which is already visible during construction in the period between the completion of the earthworks and the permanent covering of the slope with vegetation. The proper protection of a slope surface should combine an anti-erosion function with the possibility of improving soil moisture content conditions—irrigation or drainage. For this purpose, three-dimensional geocellular systems made of non-biodegradable materials with long-term durability (polyethylene) are being used more and more frequently. An interesting solution is the use of Kemafil ropes, based on which 3D geosynthetics are produced which resemble honeycomb in shape [46].

An innovative technology in the use and production of geosynthetics that allow the use of natural waste materials is Kemafil geosynthetic georopes. Kemafil georope production technology was developed in the late 1970s and can achieve thicknesses reaching up to 150 mm. Kemafil ropes may have cores made of various substances, including waste materials, e.g., wool or shredded textile waste, which are placed in a special biodegradable coating [40,47]. The casing of Kemafil ropes can be any type of material—jute fabric, jute mesh, needle-punched non-woven fabric, e.g., wool, or stitched from waste fibres with grass seeds (if they are used as a biodegradable material). Cotton or sisal rope can be used as a braid. Broda et al. [36,47] and Grzybowska-Pietras et al. [46,48], as well as

Nguyen et al. [49], used Kemafil ropes made of non-woven wool fabric in their research as an element of the anti-erosion protection and reinforcement of slopes. These ropes were laid in a meandering form or in the form of a grid, constituting an effective system protecting the slope surface. Based on the analysis of research conducted on experimental plots, Grzybowska-Pietras and Juzwa [50] showed that the use of wool non-woven ropes with a surface weight of 390 g m^{-2} and a thickness of 6 cm on the surface of slopes allows the anti-erosion function to be combined with the improvement of water balance within a slope.

The use of wool and wool waste becomes an important aspect of their proper management. Every year, huge amounts of wool waste are deposited in landfills, the use of which, according to research, can be profitable from a waste management point of view. This type of waste, apart from earth construction applications [3,40], can also be used in technologies related to the production of building materials and concrete [51,52]. The use of waste to produce concrete, due to the low cost of obtaining wool, also becomes an important element of sustainable management in construction. Alyousef et al. [53] demonstrated the possibility of using sheep wool fibres for the production of concrete. By assessing the mechanical and microstructural properties, these authors showed that the addition of 70 mm long sheep fibres in amounts ranging from 0 to 1.5% reduced the slump values of fresh concrete. The use of sheep wool fibres reduced the compressive strength of concrete mixtures, but improved the tensile and bending strength of concrete. Interesting results were obtained by Awal and Mohammadhosseini [51], who used carpet fibres and palm oil ash as partial replacements for Portland cement in the production of concrete. By adding from 0 to 1.25% of 20 mm long carpet fibre, they obtained high tensile and bending strength, thus increasing the plasticity of concrete with higher energy absorption and better crack distribution. Their research revealed that this type of waste can be potentially applied in the production of "green" concrete.

The range of wool geotextiles used in earthworks mainly includes cover mats and nets made of wool ropes [54]. Mats are mainly used to protect grass seeds [55]. They ensure minimal evaporation and provide excellent thermal protection and an appropriate microclimate for seed germination. Wool geotextiles buried in the ground are exposed to the action of microorganisms—bacteria and fungi—that use the fibres as a source of nutrients [56–58]. During degradation, they release nutrients that become available to plants. The mats are mainly applied where rapid plant growth is required. Wool georopes are used for soil protection as materials intended for erosion control or land reclamation [38]. The biological degradation of wool is slow [59]. The hydrophobic surface of wool, its compact structure, the large number of disulfide and hydrogen bonds, and other salt stabilizers hinder the growth of bacteria and fungi and delay enzymatic hydrolysis. The husks present on the surface of the fibres create irregularities that make it difficult for microorganisms to adhere [60]. Wool absorbs large amounts of water in a way that hinders its use by microorganisms. At the same time, by absorbing water, the fibres make the microclimate around them less favourable for the development of microorganisms [61].

The influence of environmental factors on wool degradation is crucial for geotextiles designed for erosion control. Such geotextiles are usually used as short-term slope protection in the early stages of development of protective vegetation. Geotextiles installed in the soil provide immediate protection and then, through gradual decomposition, deliver organic matter and nutrients to the soil, accelerating the growth of vegetation. Geotextiles should maintain their protective potential for several weeks until the vegetation takes over the protective function [62].

Assessment and monitoring of phenomena occurring in the ground and in geosynthetics as a result of water flow is increasingly being carried out using electrofusion techniques. Geophysical methods are successfully used to solve a number of problems related to the assessment of the condition of the soil and water environment [63], to assess the technical condition of engineering structures [64,65] or to assess soil porosity and moisture content [66]. Geophysical research using electrical resistance, electromagnetic or seismic

methods involves measuring the physical properties of rocks and soils, usually from the Earth's surface, without disturbing the ground structure. In the widely used electrofusion method [67], it is assumed that the tested materials are characterized by the ability to conduct electric current. This ability depends on the moisture content and water saturation of the pores of the tested medium and the impurities in the water, especially salt compounds.

The use of wool for the production of Kemafil georopes is an ecofriendly solution for the management and use of wool waste, and activities related to the use of geogrids in the broader geo-engineering field are in line with the fundamental principles of sustainable environmental resource management.

3. Materials and Methods

The scope of this work included laboratory and field tests and numerical calculations. The laboratory tests included the basic characteristics of the Kemafil georopes used in the experiment, as well as tests of their water permeability in the vertical and horizontal directions. The georopes were prepared by the Institute of Textile Engineering and Polymer Materials of the University of Technology and Humanities in Bielsko-Biała (Poland). The grain size composition of the soil constituting the base of the experimental testing site was determined using the combined sieve–aerometric method up to a depth of 1.0 m [68]. The filtration coefficient of soil taken directly from the bottom of the excavation prepared for the installation of the georopes was determined using the variable-gradient method in an oedometer [69] on samples with a diameter of 7.5 cm and a height of 1.9 cm. The permeability coefficient tests were carried out on soil with a grain size of less than 5.0 mm.

The laboratory tests of the water permeability of Kemafil georopes were carried out in a prototype apparatus (Figure 1). The constructed apparatus enabled testing the water permeability coefficient of georopes with diameters of up to 10 cm. Taking into account the high compressibility of the ropes under load, the tests took into account the change in their diameter. Therefore, the georopes were placed in pipes of different diameters, which allowed us to determine the relationship between water permeability and the bulk density of the georope. The tests were carried out with a variable hydraulic drop when water seeped through the georope sample from top to bottom.

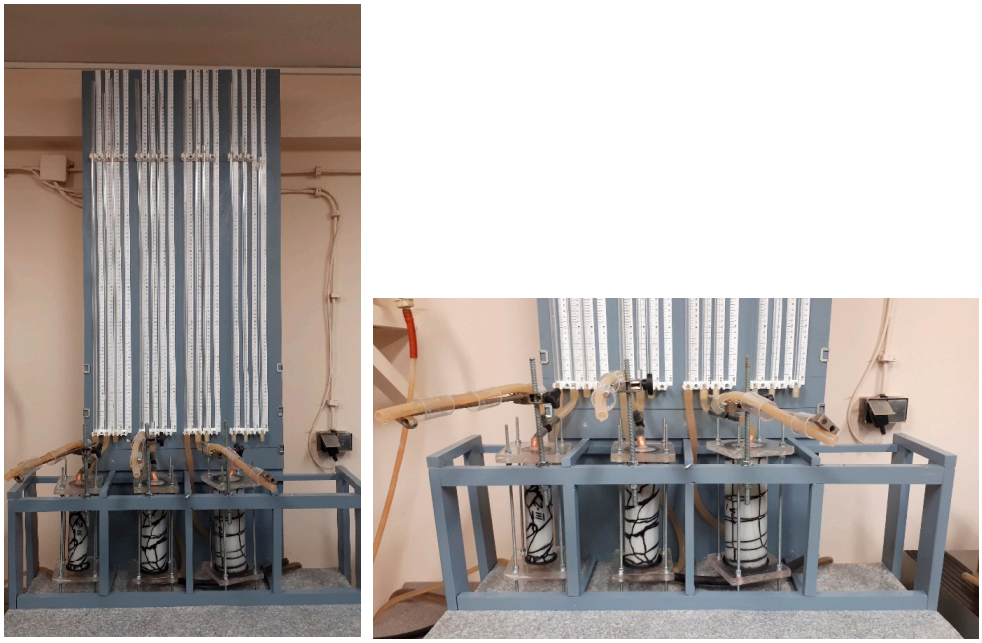

Figure 1. General view of the apparatus for determining the coefficient of permeability of Kemafil georopes (photo: A. Gruchot).

As part of the field research, penetration drilling was carried out in the subsoil of the experimental site located in Kowaniec (Poland) up to a depth of 1.0 m. During drilling, soil samples were taken for laboratory tests. Additionally, during the installation of the georopes, the soil bulk density was determined directly in the trench using the cutting ring method, which allowed to determine the porosity of the soil in the vicinity of the georopes.

The field tests at the experimental site were aimed at demonstrating the scope of changes in the moisture content of the georope and the subsoil related to water infiltration through the georopes. The tests were performed for three rows of 1.0, 2.0 and 5.0 m long georopes at a depth of 0.3 m with an inclination of 5% at a spacing of 1.0 m (Figures 2 and 3a). Wells with a diameter of 0.40 m were installed on each georope row—a supply well, through which water was supplied to the georope, and a final well (Figure 3b–d). The outlet of the georope from the supply corresponded well to the depth of its installation and was approximately 0.25 m above the bottom of the well. The bottom and the outlet of the georope from the supply well were sealed (Figure 3d).

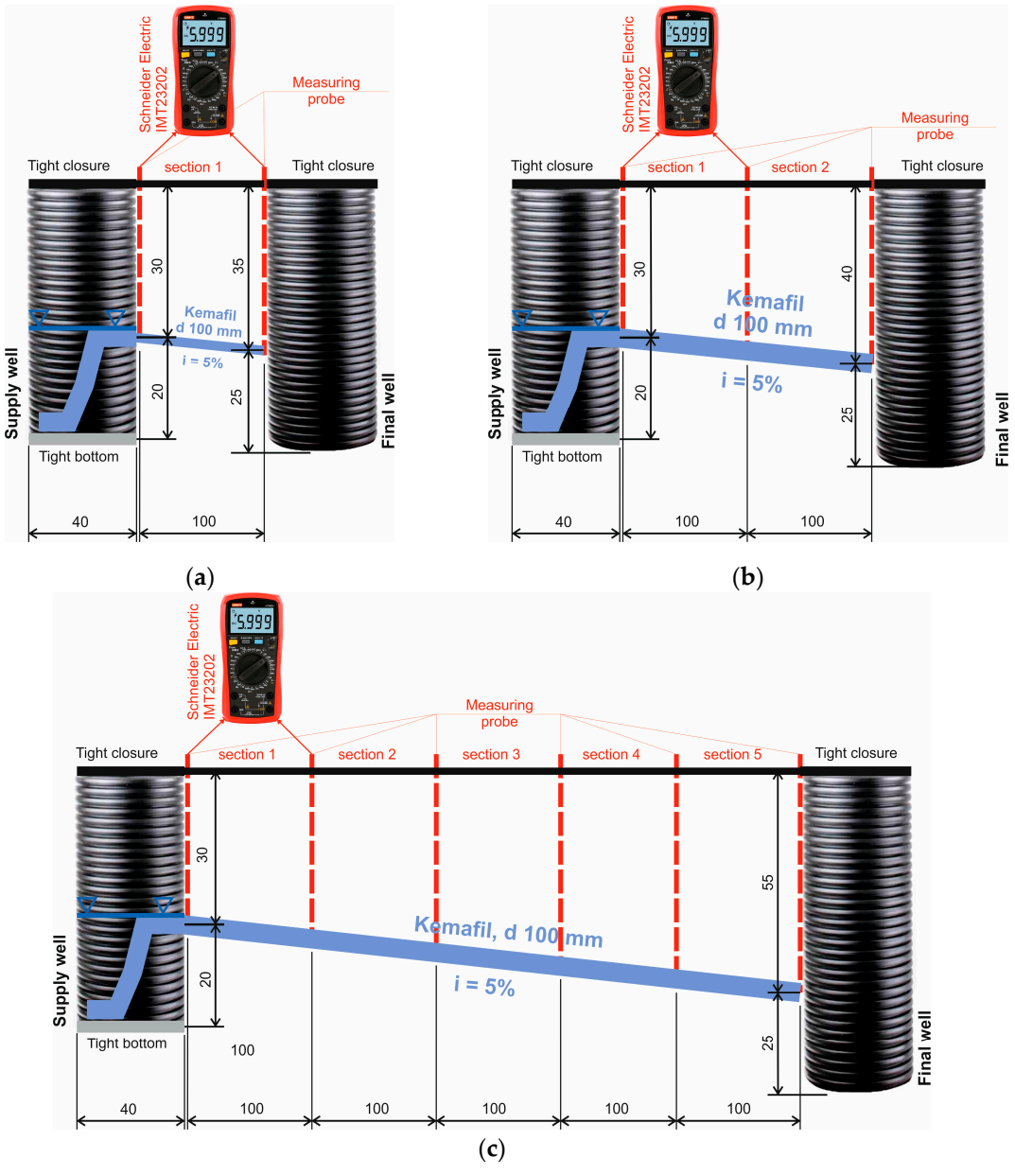

Figure 2. Diagram of the construction of the georope rows: (**a**) 1.0 m long; (**b**) 2.0 m long; (**c**) 5.0 m long.

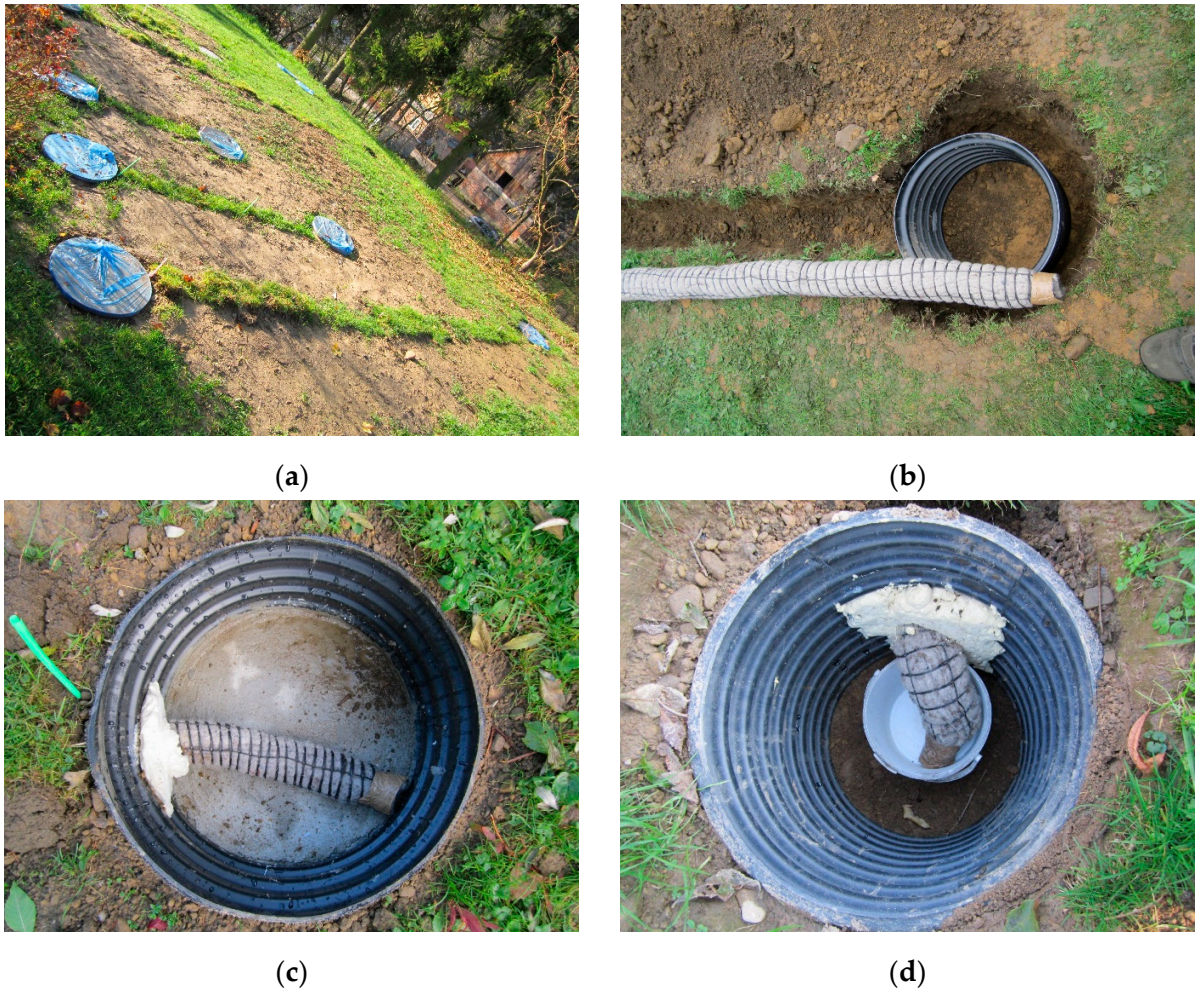

Figure 3. Elements of a drainage system made of Kemafil georopes (photo by M. Cholewa): (**a**) general view of the experimental plot; (**b**) view of the Kemafil georope before installation in the soil; (**c**) supply well; (**d**) final well.

Geophysical surveys are included in the group of non-invasive methods and are helpful in ground investigations because they do not disturb the structure of the soil. Data from this type of survey are obtained by means of spatial sampling. Traditional surveys (drilling and excavation) cause damage to the soil structure and many times require additional testing. As indicated by the research of Tabbagh et al. [71], the use of geophysical surveys in correlation with laboratory tests contributes to increasing the level of soil interpretation. Laboratory geotechnical testing has clearly shown that electrical resistivity varies with moisture content and grain size composition. As moisture content and fine content increase, the electrical resistivity values of soils decrease. Similarly, de Jong et al. [72] note the significant relationship between soil resistivity and changes in soil moisture. The use of electrical resistivity tomography makes it possible to determine the spatial dynamics of soil moisture distribution, although the field experiments do not yield accuracy similar to laboratory experiments.

Changes in the moisture content of the geogrid were determined using the electrical resistivity method, based on changes in its resistance using measuring probes installed at 1 m intervals in each drainage section (Figure 2). The probes were installed directly in the georope, and the section in the ground was insulated. Resistance measurements were performed every 10 min using a Schneider Electric IMT23202 multimeter (Figure 4) which measured the resistance in the range of up to 200 kΩ. The multimeter measured the resistance every 1 s over 10 s, giving the final result as the mean of 10 reads. Resistance

measurements were performed for two adjacent probes. During this study, the volume of infiltrating water from the supply well into the georope was also recorded. Before starting the resistance measurements, the supply well was filled with water up to the upper edge of the georope, and then the water in the well was refilled to this level every 10 min, recording the volume of added water. Nine measurement cycles of 120 min each were carried out monthly from October 2020 to June 2021 (Table 1). During the measurements, the temperature of air and water in the supply well was also recorded using multimeter probes, and the soil moisture content was assessed macroscopically [70].

Figure 4. View of the Schneider Electric IMT23202 multimeter used to measure the resistance of the Kemafil georope (photo by A. Gruchot).

Table 1. Characteristics of weather conditions during research.

Measurement Date	Temperature [°C]			Moisture Content Based on Macroscopic Analysis	Type of Precipitation and Its Intensity Within 24 h Before Measurement
	Air	Water	Soil		
7 October 2020	12	5	3	moist	snow/constant
18 November 2020	6	2	4	slightly moist	rain/poor
15 December 2020	−1	0	0	moist	snow/poor
5 January 2021	−4	0	−2	moist	lack
17 February 2021	−2	0	−1	moist	snow/fleeting
13 March 2021	−1	0	0	moist	snow/poor
1 April 2021	20	3	4	slightly moist	lack
11 May 2021	15	4	5	moist	rain/fleeting
8 June 2021	22	3	3	wet	rain/intense

Shallow non-invasive geophysics (electrical resistivity tomography) is an increasingly common method used to identify the soil–water conditions in the subsoil. If these analyses are additionally supported by the study of grain size composition, it is possible to determine the variability of the geological structure indicating the occurring glacitectonic disturbances [73]. Measurements of the electrical resistivity of soils together with drilling were also applied in the shallow geotechnical reconnaissance of an experimental flood

bank in Czernichów village (Poland) near the Vistula River [74]. On the basis of geoelectric surveys, quantitative information was obtained about the alluvial soil layers (sands, gravels and clays) present in the subsoil. The correlation between the data obtained from the geoelectric and geotechnical surveys allowed a much better identification of the geological structure of the subsoil.

As part of the field research, the filtration properties of the soil in the subsurface zone of the experimental plot were also determined. The soil coefficient of infiltration was tested at a depth of 0.20 m using the Saturo automatic infiltrometer (Figure 5). In this device, unlike in typical infiltrometers, water infiltrates into the ground through a single cylinder. This type of solution causes water infiltration into the soil to occur partly vertically and partly horizontally. In order to limit the influence of side infiltration on the assessment of the infiltration coefficient values, two values of water pressure in the cylinder were used.

Figure 5. View of the research station for testing the infiltration coefficient with the Saturo infiltrometer (photo by M. Cholewa).

Based on laboratory and field tests, calculations of water flow in georopes were made using the finite element method in the GeoStudio (v. 2020) software. The purpose of the calculations was to analyze the process of water redistribution in the subsoil near the georope. A two-dimensional model of the soil medium was adopted for the calculations, with a calculation mesh size of 1 × 1 cm, georope and subsoil to a depth of 0.35 m below ground level, and 2 × 2 cm of substrate under the georope (Figure 6) to a depth of 2.0 below ground level. The water level in the well during the analysis was considered as a boundary condition. The calculation results were verified by analyzing changes in the degree of saturation, pore pressure in the georope and the subsoil, and water velocity in the georope. A 5.0 m long georope was used for modelling. In the numerical calculations, in accordance with the field research methodology, it was assumed that water was supplied to the supply well over two hours. The next two hours of numerical modelling were intended to demonstrate changes in the wetting zone due to the lack of water supply to georopes.

The calculations adopted the composition of the subsoil from field tests. The calculations conducted for the soil in the near-surface zone and in the vicinity of the georope adopted the mean value of the coefficient of permeability from field tests with the Saturo infiltrometer, while for the soil below the georope, the coefficient of permeability was half an order of magnitude lower. This was due to the fact that below the depth of the georope installation there was silt soil with gravel and sand, with a slightly higher density. The retention curve was adopted for silt soils, as proposed in the GeoStudio programme. In numerical calculations, the selection of georope retention parameters became problematic. There is no information in the literature regarding the retention properties of sheep fibres, but there are data regarding substrates containing mineral fibres [75], or soils containing

mineral fibres [76]. The results of the laboratory tests and field observations showed that Kemafil georopes were characterized by high water absorption, similar to peat soils. Therefore, for the purposes of numerical calculations, the parameters of the van Genuchten equation [77] given by Cannavo et al. [78] were adopted as follows: $\alpha = 17.96$ kPa^{-1} and n = 2.0.

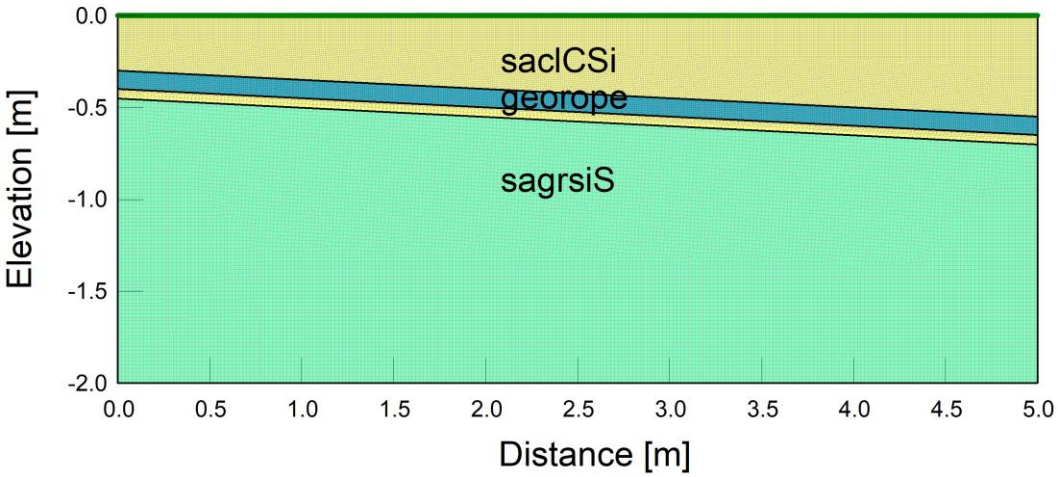

Figure 6. Discretization of the numerical model of the subsoil with a built-in georope.

The research results were analyzed using Microsoft Excel (v. 2019), as well as the Google Colaboratory platform [79], with the following Python libraries: numpy (v. 1.26.4) [80], pandas (v. 2.2.2) [81], matplotlib (v. 3.7.1) [82] and seaborn (v. 0.13.2) [83]. The first two libraries were used to analyze and process the measurement data, while the latter two were used to visualize the research results.

4. Results

The tests were conducted using Kemafil georopes with a diameter of 100 mm and a core made of rolled non-woven fabric from wool waste without lagging, only with a string braid (Figure 7). The georope was characterized by a narrow range of diameter changes, i.e., from 10.0 to 10.3 cm, and its natural bulk density ranged from 0.0598 to 0.0634 g cm^{-3} (mean of 0.0612 g cm^{-3}).

(**a**) (**b**)

Figure 7. View of the 100 mm diameter Kemafil georope used in the study (photo by A. Gruchot): (**a**) cross section of Kemafil georope; (**b**) top view of the Kemafil georope, visible a string braid.

The tests of the hydraulic properties of Kemafil georopes after their application in the ground were carried out at the experimental site located in Kowaniec (Poland). The geotechnical reconnaissance showed that the subsoil of the experimental site is composed of silty soils with gravel, the content of which increases with depth. Multi-fraction (C_U = 40.3, C_C = 1.14) clayey coarse silt with sand (saclCSi) occurred up to a depth of 0.40 m (Figure 8). Further below, up to a depth of 1.0 m below the ground surface there was multi-fraction (C_U = 160.4) silty soil with gravel and sand (sagrsiS) [84]. However, directly at the depth of the georope installation, there was multi-fraction (C_U = 55.0) sandy coarse silt with gravel (grsaCSi). The grain composition in the subsoil under the georope was dominated by the sand fraction, the content of which was almost 37%; the gravel fraction content reached almost 22%, while the silty fraction was 35%, and the clay fraction content equaled 6%. During penetration drilling, the groundwater table was not found.

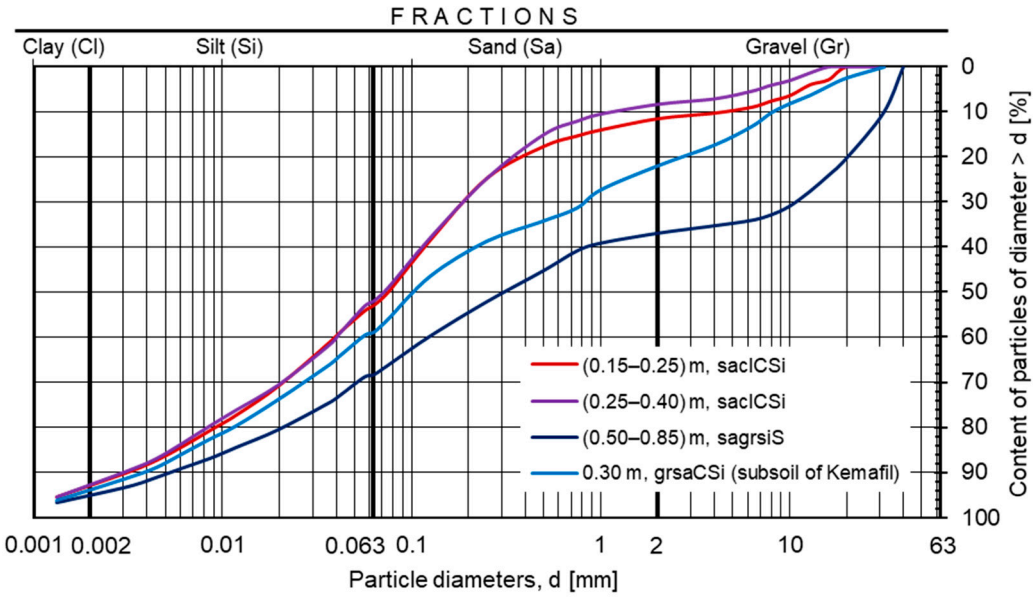

Figure 8. Grain size curves of the subsoil at the experimental site.

The bulk density of the soil was 1.92 g cm^{-3} up to a depth of 0.25 m with a moisture content of approximately 20 to 22%, and the porosity of 0.40. However, the bulk density at a depth of 0.30 m at the feeding well was 1.80 g cm^{-3} with a moisture content of just over 23%, which corresponded to a dry density of 1.45 g cm^{-3} and a porosity of 0.46.

4.1. Hydraulic Properties Tests

The determination of the coefficient of permeability of soil collected from the bottom of the excavation was carried out in an oedometer on four samples of soil. The bulk density of the samples ranged from 1.77 to 1.82 g cm^{-3}, and the moisture content was close to 25%. The values of the coefficient of permeability ranged from 1.21 $\times$ 10^{-8} m s^{-1} to 1.07 $\times$ 10^{-7} m s^{-1} (Figure 9a), and its mean value from four tests was 3.04 $\times$ 10^{-8} m s^{-1}.

On the other hand, the soil infiltration coefficient at the experimental ground, determined with an infiltrometer, ranged from 7.03 $\times$ 10^{-6} m s^{-1} to 5.40 $\times$ 10^{-5} m s^{-1} (Figure 9b). The numerical analysis was conducted using its mean value, which was 1.84 $\times$ 10^{-5} m s^{-1}. Compared to the values of the substrate soil coefficient of permeability from oedometer tests, the coefficient of permeability was three orders of magnitude higher.

The results of the laboratory tests of the water permeability of the georope showed that its coefficient of permeability depended on the bulk density and decreasing porosity (Figure 10), but the range of values was not large. Similarly, the difference between the coefficient of permeability in the vertical and horizontal directions was negligible. The mean value of the coefficient of permeability of the tested georope in the vertical direction was 4.12 $\times$ 10^{-3} m s^{-1}, and in the horizontal direction it was 4.99 $\times$ 10^{-3} m s^{-1}. It should

be noted that these values are higher than the requirements for materials used for filtration layers and seepage layers in road surface structures [85]. On the other hand, these values are almost one and a half orders of magnitude smaller than the values of the filtration coefficient given for wool textile covers in the direction perpendicular to the product [40], whereas it should be noted that these tests were carried out without sample load. Similar values are reported by Marczak et al. [45] for wool geotextiles, at the same time showing that the water permeability of these materials increases as a result of their biodegradation.

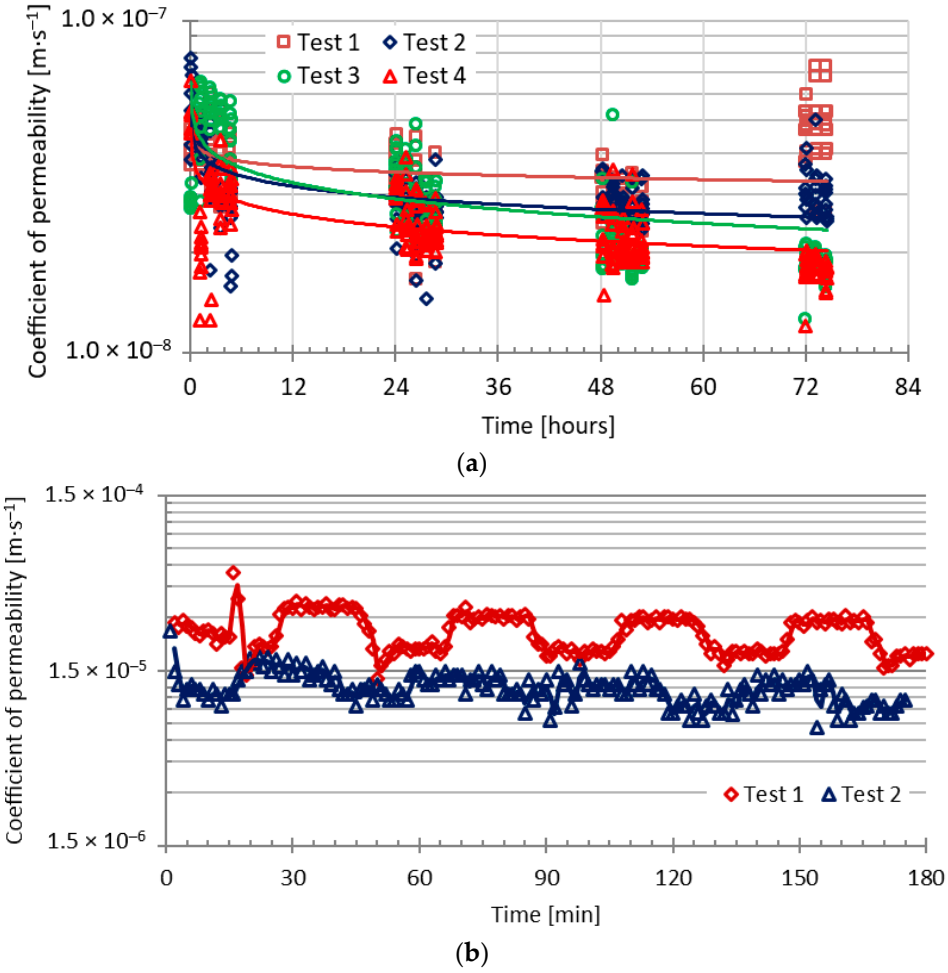

Figure 9. Results of the water permeability tests of the subsoil at the experimental ground: (**a**) coefficient of permeability from oedometer, sampling depth 0.30 m; (**b**) coefficient of infiltration from infiltrometer, ring installation depth 0.20 m.

In the conducted experiments, the use of georopes for drainage was less important, and therefore the criterion of clogging of the georope material was not introduced. It was assumed that the georope material would initially function only as seepage drainage, and later would undergo biodegradation, thus increasing the nitrogen content in the soil and causing faster growth of the slope-stabilizing vegetation.

By comparing the value of the filtration coefficient obtained from subsoil tests using the Saturo infiltrometer with the georope filtration coefficient from laboratory tests, it can be concluded that the hydraulic conductivity criterion (Equation (5)) was met because:

$$\left(k_s^{gt} = 4.12 \times 10^{-3}\ \mathrm{m\ s^{-1}}\right) > (\gamma = 1.0)\ \left(k_s^{s} = 1.84 \times 10^{-5}\ \mathrm{m\ s^{-1}}\right) \quad (6)$$

The empirical coefficient γ was adopted as for less critical applications [9].

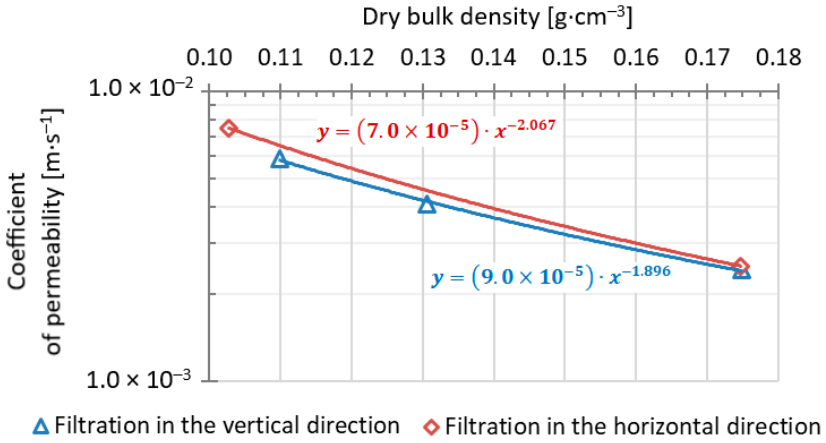

Figure 10. Changes in the georope coefficient of permeability depending on its bulk density.

4.2. Resistance of Georopes

The resistance tests of Kemafil georopes were carried out in nine measurement series of 120 minutes each in monthly cycles over the period from October 2020 to June 2021. The recorded meteorological conditions were typical for the period from autumn to spring for the climatic conditions of Poland. The air temperature during tests ranged from −4 to 20 °C with varying amounts of precipitation (Table 1). The air temperature was measured at the ground and despite the occurrence of short periods of negative temperatures, no ground freezing was observed. Figure 11 shows the depth of precipitation and the thickness of snow cover recorded at the Kowaniec meteorological station [69] in the period from October 2020 to July 2021. The weather conditions during the research period varied. There was rainfall in the period preceding the first and last measurement cycles. On the other hand, in the case of the fifth and seventh measurement cycles, snowfall was recorded at the meteorological station. Tap water with a temperature ranging from 0 to 5 °C was used for the tests.

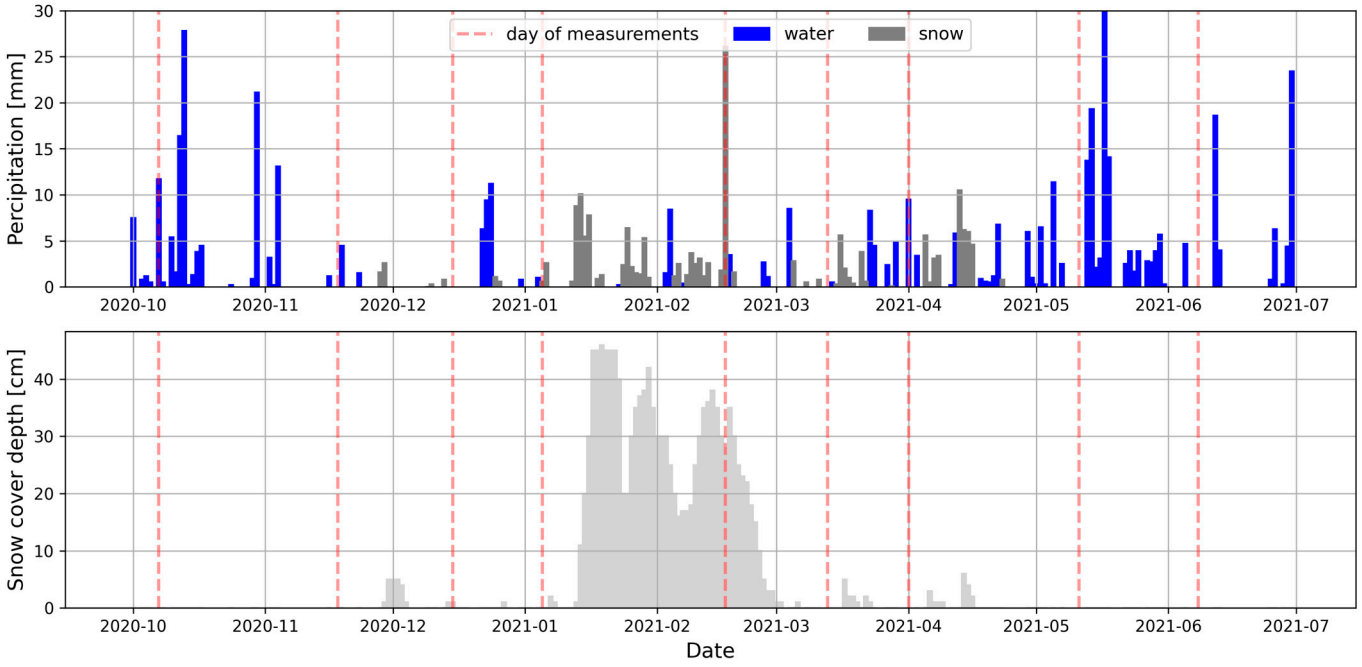

Figure 11. Meteorological conditions during the research period from the Kowaniec station of the Institute of Meteorology and Water Management (own study, after [86]).

By extending the implementation time for all three georope sections, the volume of supplied water decreased on average from 15 dm^3 to 5 dm^3 per each subsequent 10 min of testing (Figure 12a), indicating the increasing saturation of the georope. This phenomenon is typical in flow conditions in the unsaturated zone of porous media. The mean volume of infiltrating water was just over 9 dm^3, with a mean standard deviation of 2.3 dm^3. It should be noted that during each 120 min measurement cycle, no water outflow was observed in the final well, regardless of the length of the georope. This indicates water infiltration from the georope into the ground profile.

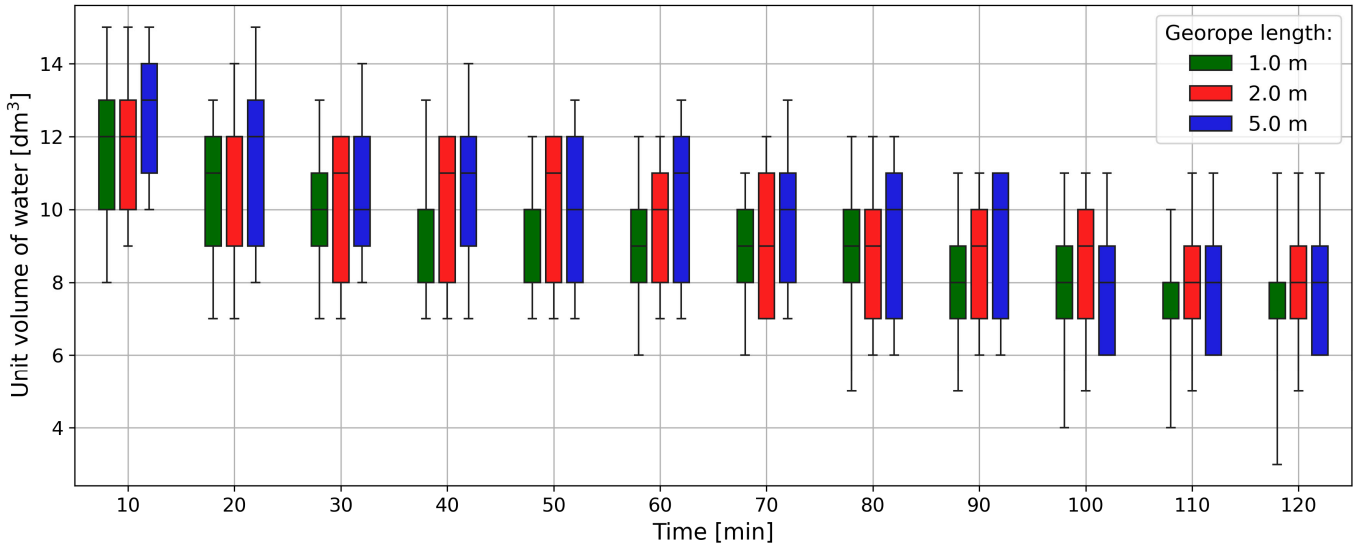

(**a**)

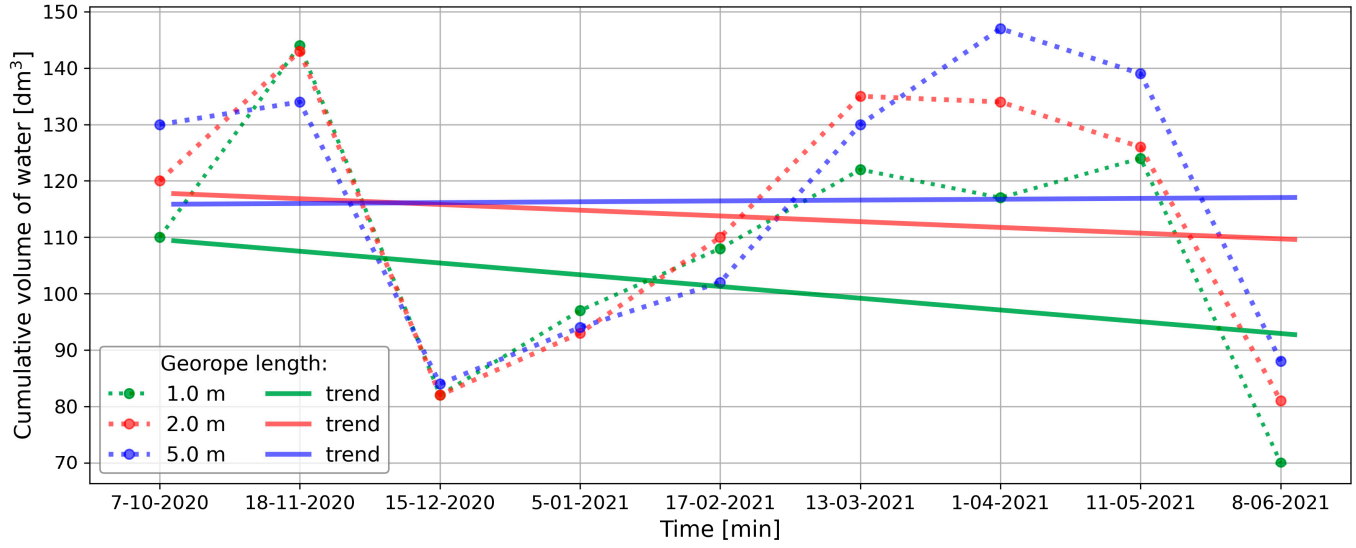

(**b**)

Figure 12. Changes in the unit (**a**) and cumulative (**b**); volume of water during the measurements (**a**) and the entire test cycle (**b**).

The cumulative value of the volume of water flowing from the supply well during a 120 min measurement cycle ranged from 70 to 147 dm^3 (Figure 12b), averaging 110.5 dm^3 with a mean standard deviation of 22.4 dm^3. A significant reduction in the volume of infiltrated water was found during the measurement cycle in December 2020 and June 2021. This can be explained by the low air and ground temperature and snowmelt in the first date and the occurrence of intense precipitation in the latter date (Table 1).

The water infiltration coefficient into the georope was calculated based on measurements of the volume of water flowing from the supply well. This parameter was expressed as the ratio of the volume of water to the cross-sectional area of the georope and to the measurement time. Similar values were found for individual sections of the georope. The range of values of the infiltration coefficient determined in this way ranged from 6.37×10^{-4} m s^{-1} to 3.18×10^{-3} m s^{-1} (Figure 13) with an average of 2.00×10^{-3} m s^{-1} and a deviation standard equal to 4.83×10^{-4} m s^{-1}.

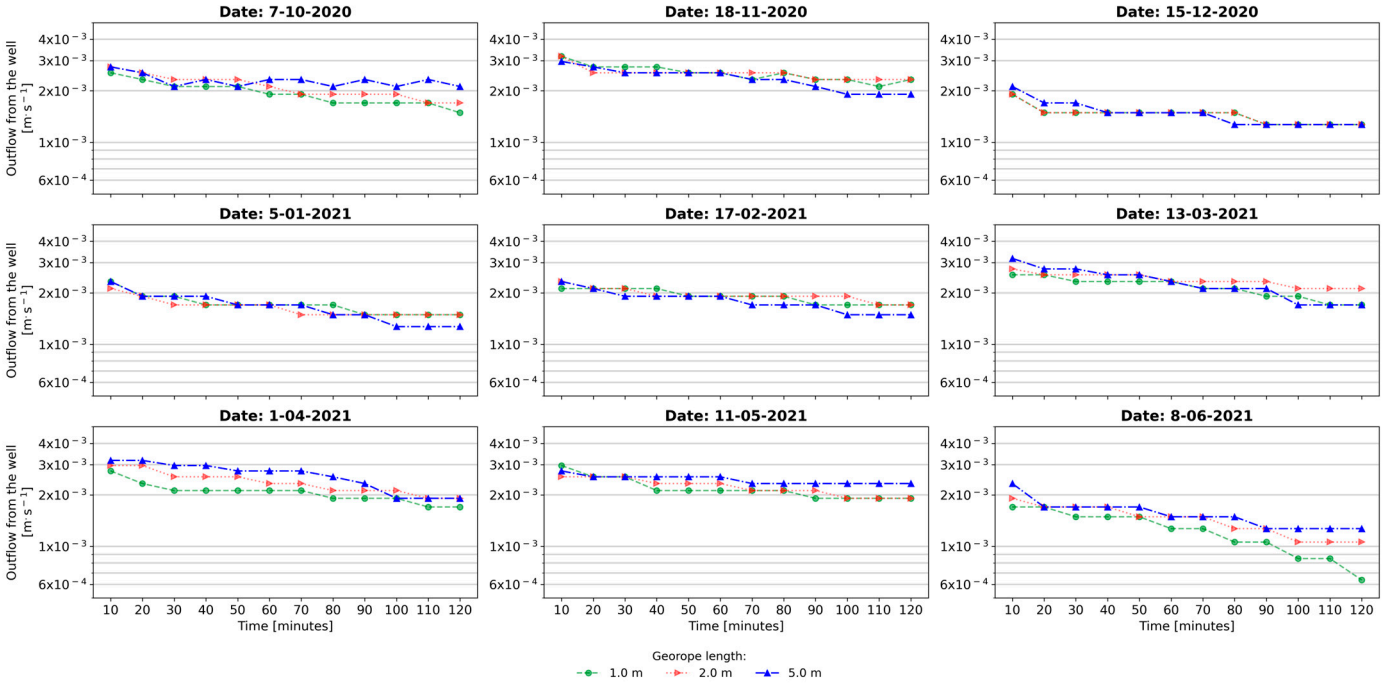

Figure 13. Changes in the velocity of water outflow from the supply well to the georope during the field tests.

Assuming that the georope carries water through its full cross-section without losses resulting from water outflow into the ground, the obtained value of the average infiltration coefficient allowed us to determine that after approximately 9, 17 and 41 min for the 1.0, 2.0 and 5.0 m long georopes, respectively, the water should flow to the final well. The calculations also showed that after the time indicated above, the water flow in the final well should be close to 8, 16 and slightly over 39 dm^3 for the georope lengths of 1.0, 2.0 and 5.0 m, respectively. As already noted, the water outflow in the final well was not found during field tests, even though the determined filtration coefficient of the georope was significantly higher by five orders of magnitude than that of the ground, and water flow through the georope could be expected. The georope used in this research did not have a rigid core and was susceptible to deformation. After its installation, this could have resulted in a significant reduction in its cross-sectional area due to soil loading, and thus could have caused an additional reduction in the water flow speed along its length.

The results of the resistance measurements showed that its value varied within quite a wide range, from 26 to 185 kΩ, and depended on the length of the georope, as well as the date of the test and its duration (Figures 14–16). In the case of the 1.0 m long georope, the range of changes in its resistance value ranged from 26 to 150 kΩ, with the highest resistance values recorded at the initial time of the study. It can also be indicated that with each subsequent measurement cycle, the initial resistance was higher and higher, and its maximum values were obtained in April 2021. As the test time was extended and the volume of water supplied increased, the range of georope resistance change decreased from 3 to 67 kΩ. The obtained trend of resistance changes indicates the occurrence of water flow

in the first section (0.0–1.0 m) of the georope as well as the possibility of water retention by the georope.

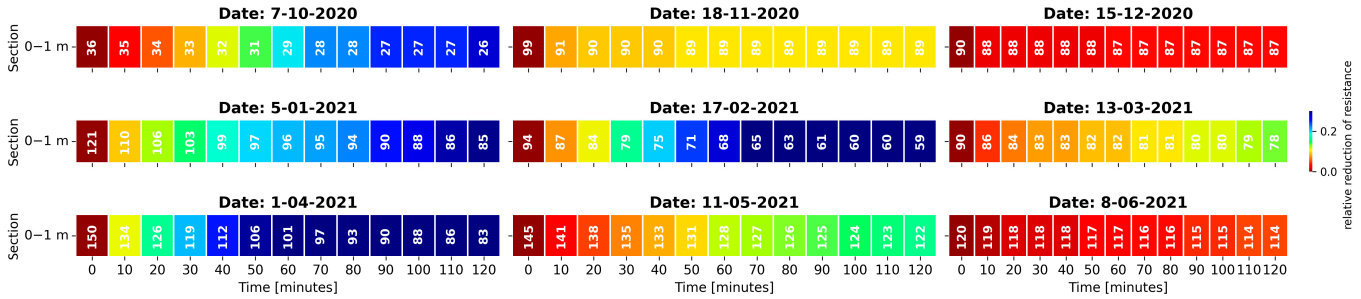

Figure 14. Changes in the resistance values of a 1.0 m long georope during measurement cycles (cells show resistance values in kΩ).

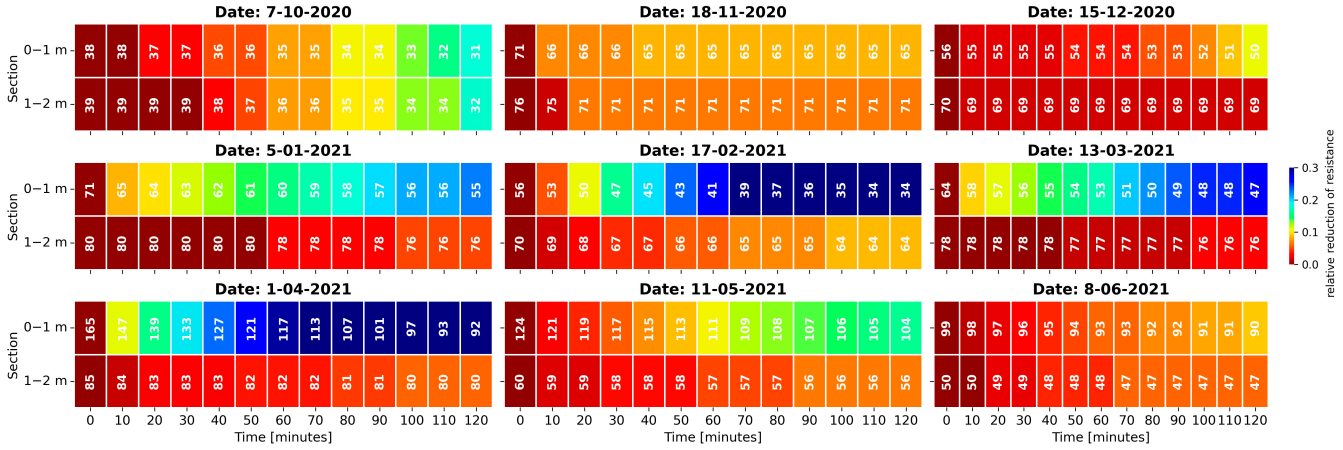

Figure 15. Changes in the resistance values of a 2.0 m long georope during measurement cycles (cells show resistance values in kΩ).

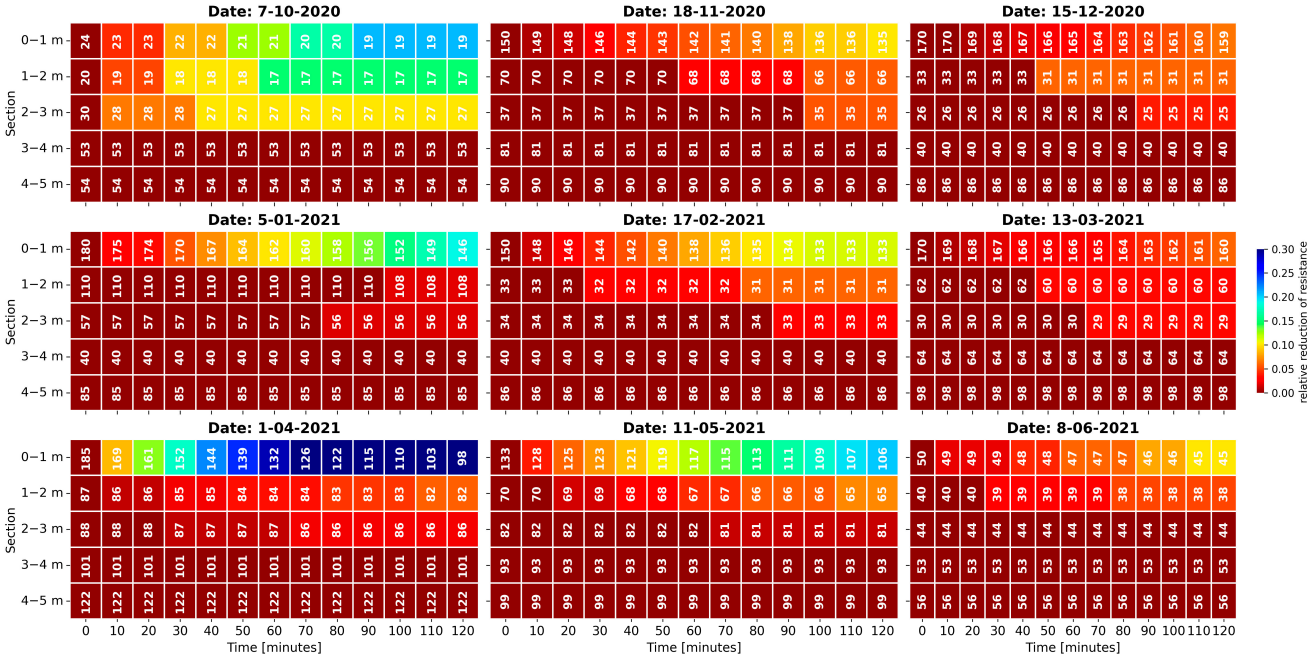

Figure 16. Changes in the resistance values of a 5.0 m long georope during measurement cycles (cells show resistance values in kΩ).

In the case of the 2.0 m long georope, the obtained resistance values ranged from 31 to 165 kΩ. The largest changes in resistance occurred on the 0.0–1.0 m section of the georope and, for example, for the measurement series carried out in April 2021, they amounted to 73 kΩ. For a georope section of 1.0–2.0 m, the resistance decreased by 7 kΩ. For this georope length, much lower resistance values were found in the initial measurement cycles compared to the last cycles. Changes in resistance during each measurement cycle indicate that there was water flow in the georope along its entire length, and it was most visible in the measurement section of 0.0–1.0 m.

In the case of the 5.0 m long georope, the changes in resistance were similar to those in the cases of the 1.0 and 2.0 m long georopes. The most significant changes in resistance were found for the first section of the georope (0.0–1.0 m), and in the further sections, the resistance changes were smaller, while in the 3.0–4.0 m and 4.0–5.0 m sections, no changes were detected. The recorded resistance changes indicate that there was no water flow through the georope in the section between 3.0 and 5.0 m. It was noticeable that in the first cycle of measurements, the georope resistance in the 0.0–1.0 m section was relatively low. In subsequent measurement cycles, apart from the last one, the resistance values in this section ranged from 133 to 185 kΩ, and for the remaining sections they were significantly lower.

As shown above, the largest changes in resistance were obtained in the section of 0.0–1.0 m for each georope length. However, the differences in resistance between individual georope lengths varied largely (Figures 14–16). This is important because the soil and water conditions of the substrate in which the georopes were installed were the same. The obtained resistance values fluctuated within quite a wide range, even within a single measurement cycle. For example, for the first measurement cycle, i.e., after embedding the georope in the ground, the resistance values during the measurements ranged from 26 to 36 kΩ for the 1.0 m long georope, from 31 to 38 kΩ for the 2.0 m long georope and from 19 to 24 kΩ for the 5.0 m long georope. The largest changes in resistance were obtained for the measurement cycle carried out in April 2021 and ranged from 83 to 150 kΩ, from 92 to 165 kΩ and from 98 to 185 kΩ for the 1.0, 2.0 and 5.0 m long georopes, respectively. The presented ranges of resistance value changes for individual georope lengths clearly indicate that the water flow in the georope was the most intense at the 0.0–1.0 m section. The differences in the obtained resistance values for individual georopes could have been caused by different degrees of deformation of the georopes resulting from their deformation after installation in the ground and the resulting change in the cross-section. This could have also been caused by variable weather conditions, mainly rainfall, during the measurements or immediately before their implementation.

It was evident that significantly smaller changes in the georope resistance occurred during the third and ninth measurement series, when the amount of water infiltrating through the ground was the smallest. On the other hand, the greatest changes in resistance were recorded in the seventh measurement series, during which the amount of water infiltration through the cord was high. Noticeable changes in resistance were also recorded in the fifth measurement series in the 1 and 2 m long georopes, despite the relatively small infiltration of water though the rope, which could have been limited due to the snowmelt occurring at that time. The obtained dependencies indicate the relationship between changes in resistance values and the size and range of infiltration in georopes.

4.3. Numerical Calculations

The results of numerical modelling allowed us to determine the potential extent of the wetting zone in the georopes during water supply to the recharge well (the first two hours) and after it was finished (the next two hours). As a consequence, changes in the degree of saturation in the georopes and in the subsoil were determined (Figure 17). The calculations also allowed us to determine the distribution of pore pressure (Figure 18); in this case, suction pressure and water flow speed in the georopes (Figure 19).

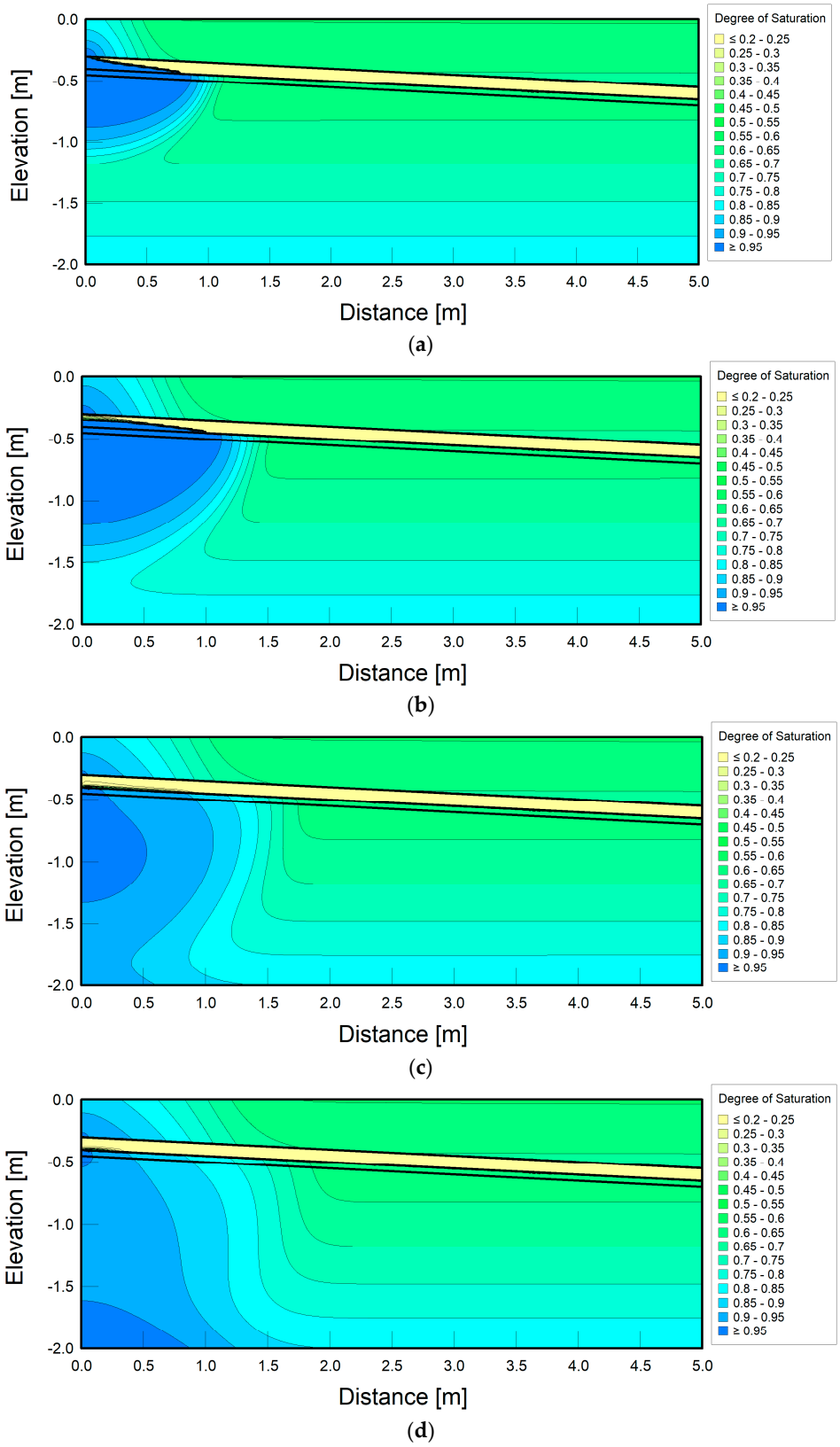

Figure 17. Changes in the degree of saturation (water wetting front) of Kemafil georopes and soil substrate: (**a**) first hour of water supply to the well; (**b**) second hour of water supply to the well; (**c**) third hour of modelling without water supply to the well; (**d**) fourth hour of modelling without water supply to the well.

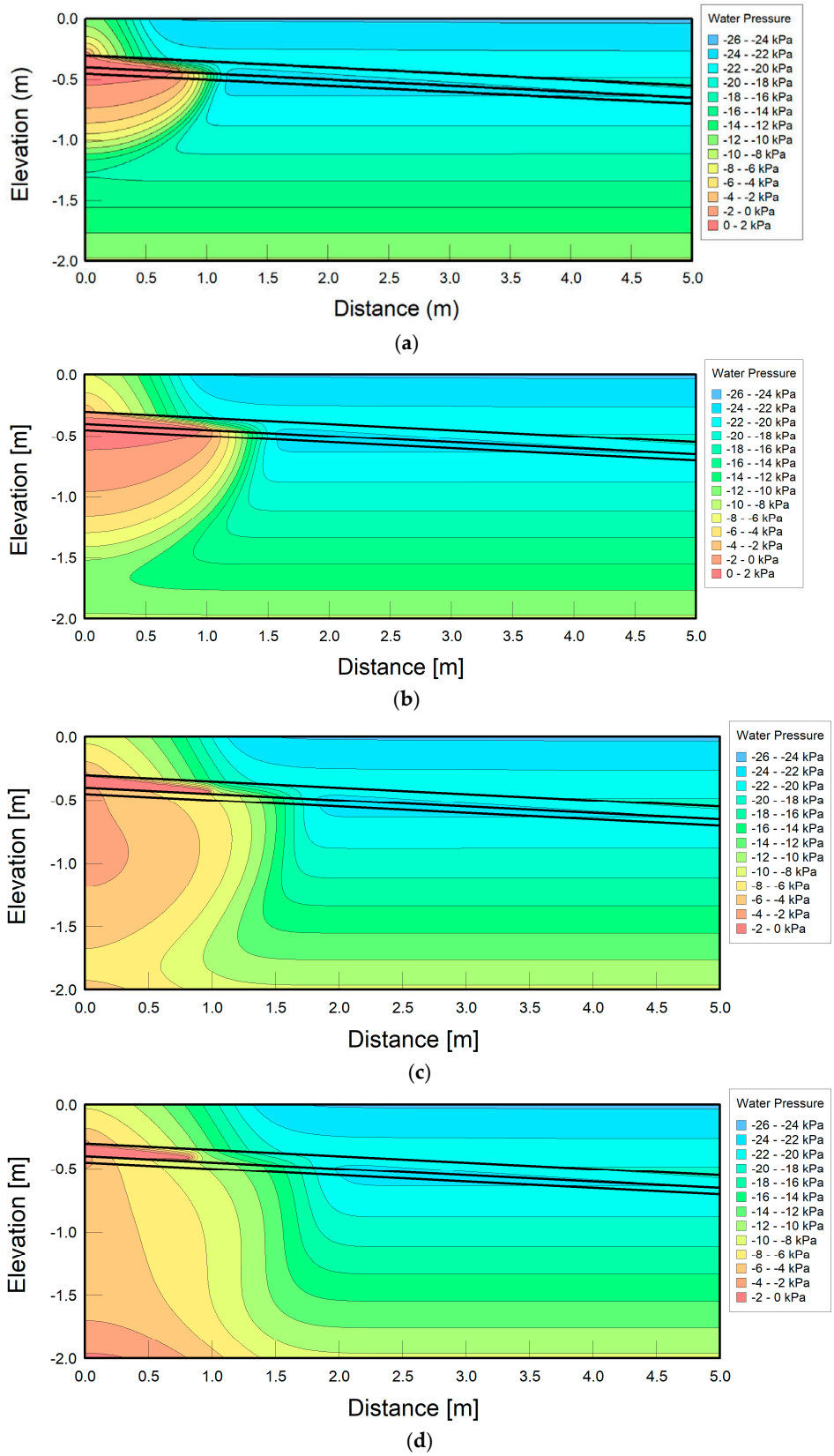

Figure 18. Distribution of suction pressure in the Kemafil georope and in the ground substrate: (**a**) first hour of water supply to the well; (**b**) second hour of water supply to the well; (**c**) third hour of modelling without water supply to the well; (**d**) fourth hour of modelling without water supply to the well.

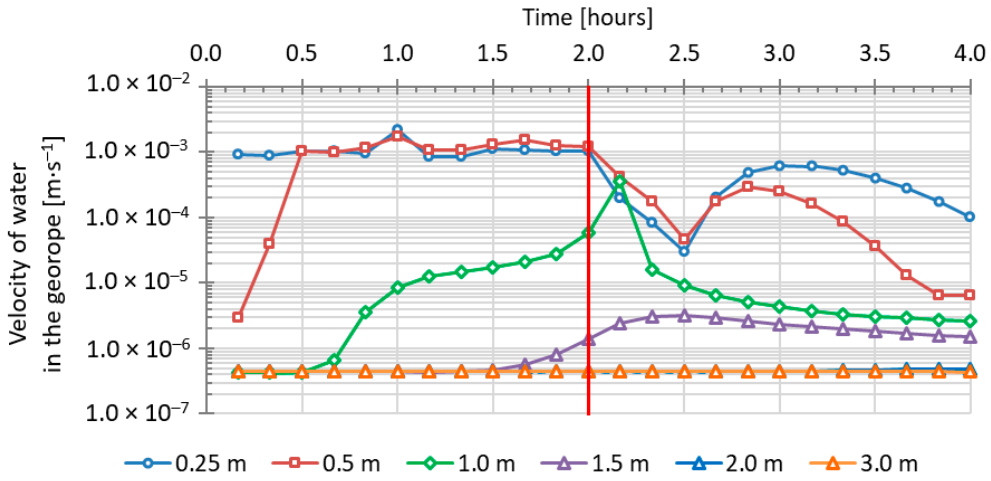

Figure 19. Results of calculations of the resulting water flow velocity in the georopes at selected lengths from the feed well outlet (the red line indicates the time until which water was supplied to the well).

The maximum value of the degree of saturation of both the georope and the subsoil (above 0.95) occurred when water was supplied to the well, at a distance from 0.0 to approximately 1.2 m, obtaining the largest horizontal range in the second hour of modelling (Figure 17a,b). The vertical range of the georope impact at a saturation degree above 0.95 of subsoil reached the maximum depth of approximately 1.2 m below ground level and it increased with an increase in the length of time that water was supplied to the well. Changes in the degree of saturation clearly indicate the water flow in the georope in its initial section. During two hours of water being supplied to the supply well, the georope was wetted mainly in its lower part, in the point of contact with the ground. The modelling results for the next two hours without water supply showed a gradual return to the initial value of the degree of saturation of the georope and the subsoil (Figure 17c,d). The degree of saturation in the section from 0.0 to 1.2 m decreased and ranged from 0.80 to 0.95. The obtained results indicate that under the prevailing soil and water conditions, water completely infiltrated the ground through the lower part of the georope cross-section.

However, the degree of saturation of the georope and subsoil in the section from approximately 1.2 to 5.0 m did not change during the calculations compared to the initial state and varied within the depth from 0.4 to 0.8 m. The obtained results indicate that in order to obtain water flow over a longer distance, the water supply time should be extended given the existing soil and water conditions. It can therefore be concluded that the obtained calculations are qualitatively consistent with the results of field measurements. On the other hand, the calculations carried out have limitations related to the use of a two-dimensional measurement system and the inability to calculate horizontal flow in the vicinity of georopes.

The process of water infiltration through the georope into the subsoil caused a change in the wetting front and thus the suction pressure (negative pore pressure) of water in the soil pores. It should be clearly stated that during the four hours of modelling of the georope operation, the suction pressure within the 0.0 to 1.0 m section was similar and ranged from 0 to −4 kPa (Figure 18). This indicates, according to the earlier analysis, that the georope was almost fully saturated. The horizontal range of suction pressure changes in the subsurface was observed within the 0.0 to 2.0 m section. On the other hand, the vertical range of suction pressure changes was observed throughout the entire ground section, i.e., up to a depth of 2.0 m above the ground level. However, the fluctuations in the suction pressure of the ground subsoil along the analyzed section of the georope were small, ranging from −10 to −4 kPa.

On the other hand, in the georope section from 2.0 to 5.0 m, there were no changes in the suction pressure during the four hours of modelling of the georope operation. In the

ground surface zone, the suction pressure was around −26 kPa, and at a depth of 2.0 m below the ground surface it was −8.0 kPa.

Figure 19 shows changes in the water flow rate in the georope at selected distances from the supply well, resulting from calculations in the vertical and horizontal directions. The red line marks the time when water was supplied to the well. An analysis of the obtained water flow velocity values indicates that this flow occurred for two full hours at a distance of 0.25 m from the well. Similarly, but with a 30 min delay, the flow occurred at a distance of 0.5 m from the well. In this case, both rates were the same and corresponded to the filtration coefficient of the georope. However, at distances of 1.0 and 1.5 m, for 30 and 90 min, respectively, the flow velocity was close to the filtration coefficient of the subsoil, indicating no water flow in the georope. After this time, the water flow rate increased. However, the obtained velocity values in the second hour of modelling were 1.5 and 3 orders of magnitude smaller, respectively, than the filtration coefficient of the georope. No water flow was found within the distances of 2.0 and 3.0 m. The obtained water flow rates were close to the filtration coefficient of the subsoil. Also interesting is the fact that after the water supply to the feed well was completed, the water velocity decreased rapidly. The conducted analysis indicates that the use of georopes for seepage drainage will be disputable.

In general, the obtained results of calculations of the water infiltration rate from the supply well (Figure 19) proved to be lower than those obtained from direct calculations, which could have been caused by the occurrence of local privileged filtration paths near the well and the georope related to soil loosening. Unlike field tests, numerical calculations showed a potential water flow over a length of 1.0 m, which theoretically should have been registered during the field test. The results of field observations did not indicate the existence of a clear water flow in the collection wells at this distance, but the flow could have been small and thus difficult to observe.

5. Conclusions

Laboratory tests of the water permeability of Kemafil georopes using geotextiles made of wool waste showed that their filtration properties correspond to well-permeable soils. The georopes were significantly more permeable than the subsoil at the experimental site, allowing us to conclude that the criterion of hydraulic conductivity—set for geosynthetics when used as filters—was met.

Field resistance tests did not confirm the high hydraulic conductivity of the georopes, similar to those obtained in laboratory tests. However, it should be clearly indicated that electrical resistance tests showed the occurrence of water flow, meaning that the georopes had water-conducting properties at least in their initial section. This research showed that the use of georopes for drainage did not meet the assumed hypothesis. Therefore, the analyzes did not take into account the criteria resulting from the use of this type of material for drainage purposes.

Field tests showed that the amount of water carried through the georopes was consistent with the results of the georope resistance measurements. This proves the usefulness of the measurement method used to observe filtration phenomena occurring in georopes. This study showed that the values and changes in the resistance of georopes varied over time and depended on the amount of water supplied and the temporary soil absorption related to the weather conditions occurring in the period before and during the measurements.

Numerical calculations showed qualitative similarity with the results of the field tests. They also indicated that a significant volume of water from the georopes infiltrated into the ground in their vicinity. This means that in the field conditions, which are complex in terms of water permeability, georopes can act as percolators for water in the ground, making it more available to plants. Taking into account the obtained research results and information provided in the literature, it should be concluded that the use of georopes made of wool waste, which is a biodegradable material, is only a temporary solution intended to support plant vegetation.

Author Contributions: Conceptualization, M.C., A.G., T.Z. and J.S.; methodology, M.C. and A.G.; software, T.Z.; validation, A.G., M.C. and T.Z.; formal analysis, M.C.; investigation, A.G., T.Z. and M.C.; data curation, M.C. and A.G.; writing—original draft preparation, A.G., T.Z. and J.S.; writing—review and editing, A.G. and T.Z.; visualization, A.G. and T.Z.; supervision, A.G. All authors have read and agreed to the published version of the manuscript.

Funding: This research received no external funding.

Institutional Review Board Statement: Not applicable.

Informed Consent Statement: Not applicable.

Data Availability Statement: Data are contained within the article.

Acknowledgments: The authors would like to thank Jan Jędrol for his help in carrying out the field tests presented in this paper. The authors would like to thank the anonymous reviewers for their efforts towards improving the manuscript.

Conflicts of Interest: The authors declare no conflicts of interest.

References

1. Journal of Laws. Dz.U.2013.21. Ustawa z Dnia 14 Grudnia 2012 r. o Odpadach. 2012. Available online: https://isap.sejm.gov.pl/isap.nsf/DocDetails.xsp?id=wdu20130000021 (accessed on 10 May 2022).
2. Diambra, A.; Ibraim, E.; Muir Wood, D.; Russell, A.R. Fibre reinforced sands: Experiments and modelling. *Geotext. Geomembr.* **2010**, *28*, 238–250. [CrossRef]
3. Hejazi, S.M.; Sheikhzadeh, M.; Abtahi, S.; Zadhoush, A. A simple review of soil reinforcement by using natural and synthetic fibers. *Constr. Build. Mater.* **2012**, *30*, 100–116. [CrossRef]
4. Patel, S.K.; Singh, B. A comparative study on shear strength and deformation behaviour of clayey and sandy soils reinforced with glass fibre. *Geotech. Geol. Eng.* **2020**, *38*, 4831–4845. [CrossRef]
5. Correia, N.S.; Rocha, S.A.; Lodi, P.C.; McCartney, J.S. Shear strength behavior of clayey soil reinforced with polypropylene fibers under drained and undrained conditions. *Geotext. Geomembr.* **2021**, *49*, 1419–1426. [CrossRef]
6. Ganiev, J.; Yamada, S.; Nakano, M.; Sakai, T. Effect of fiber-reinforcement on the mechanical behavior of sand approaching the critical state. *J. Rock Mech. Geotech. Eng.* **2022**, *14*, 1241–1252. [CrossRef]
7. Broda, J.; Rom, M.; Grzybowska-Pietras, J.; Przybyło, S.; Laszczak, R. Application of waste materials for the production of innovative geotextiles for soil protection against surface erosion. *Arch. Waste Manag. Environ. Prot.* **2015**, *17*, 135–140.
8. Rickson, R.J. Controlling sediment at source: An evaluation of erosion control geotextiles. *Earth Surf. Process. Landforms* **2006**, *31*, 550–560. [CrossRef]
9. Kalore, S.A.; Babu, G.L.S. Hydraulic conductivity requirement of granular and geotextile filter for internally stable soils. *Geotext. Geomembr.* **2022**, *50*, 510–520. [CrossRef]
10. Hong, Y.S.; Wu, C.S. Filtration behaviour of soil-nonwoven geotextile combinations subjected to various loads. *Geotext. Geomembr.* **2011**, *29*, 102–115. [CrossRef]
11. Fourie, A.B.; Kuchena, S.M. The influence of tensile stresses on the filtration characteristics of geotextiles. *Geosynth. Int.* **1995**, *2*, 455–471. [CrossRef]
12. Fourie, A.B.; Addis, P.C. Changes in filtration opening size of woven geotextiles subjected to tensile loads. *Geotext. Geomembr.* **1999**, *17*, 331–340. [CrossRef]
13. Wu, C.S.; Hong, Y.S.; Wang, R.H. The influence of uniaxial tensile strain on the pore size and filtration characteristics of geotextiles. *Geotext. Geomembr.* **2008**, *26*, 250–262. [CrossRef]
14. Palmeira, E.M.; Fannin, R.J. Soil-geotextile compatibility in filtration. In Proceedings of the Seventh International Conference on Geosynthetics, 7-Icg, Nice, France, 22–27 September 2002.
15. Markiewicz, A.; Koda, E.; Kawalec, J. Geosynthetics for filtration and stabilisation: A review. *Polymers* **2022**, *14*, 5492. [CrossRef]
16. Imanzadeh, S.; Jarno, A.; Hibouche, A.; Bouarar, A.; Taibi, S. Ductility analysis of vegetal-fiber reinforced raw earth concrete by mixture design. *Constr. Build. Mater.* **2020**, *239*, 117829. [CrossRef]
17. Gruchot, A.; Michniak, D. Compression strength of fly ash with the addition of fiber reinforcement. *Acta Sci. Pol. Form. Circumiectus* **2015**, *14*, 43–54. [CrossRef]
18. Araya-Letelier, G.; Concha-Riedel, J.; Antico, F.C.; Valdés, C.; Cáceres, G. Influence of natural fiber dosage and length on adobe mixes damage-mechanical behavior. *Constr. Build. Mater.* **2018**, *174*, 645–655. [CrossRef]
19. Sangma, S.; Tripura, D.D. Experimental study on shrinkage behaviour of earth walling materials with fibers and stabilizer for cob building. *Constr. Build. Mater.* **2020**, *256*, 119449. [CrossRef]
20. Kandemir, A.; Pozegic, T.R.; Hamerton, I.; Eichhorn, S.J.; Longana, M.L. Characterisation of natural fibers for sustainable discontinuous fibre composite materials. *Materials* **2020**, *13*, 2129. [CrossRef]
21. Sharma, V.; Marwaha, B.M.; Vinayak, H.K. Enhancing durability of adobe by natural reinforcement for propagating sustainable mud housing. *Int. J. Sustain. Built Environ.* **2016**, *5*, 141–155. [CrossRef]

22. Gowthaman, S.; Nakashima, K.; Kawasaki, S. A state-of-the-art review on soil reinforcement technology using natural plant fiber materials: Past findings, present trends and future directions. *Materials* **2018**, *11*, 553. [CrossRef]
23. Mulenga, T.K.; Ude, A.U.; Vivekanandhan, C. Techniques for modelling and optimizing the mechanical properties of natural fiber composites: A review. *Fibers* **2021**, *9*, 6. [CrossRef]
24. Parlato, M.C.M.; Cuomo, M.; Porto, S.M.C. Natural fibers reinforcement for earthen building components: Mechanical performances of a low quality sheep wool ("Valle del Belice" sheep). *Constr. Build. Mater.* **2022**, *326*, 126855. [CrossRef]
25. Parlato, M.C.M.; Porto, S.M.C. Organized framework of main possible applications of sheep wool fibers in building components. *Sustainability* **2020**, *12*, 761. [CrossRef]
26. Porubská, M.; Koóšová, K.; Braniša, J. The application of sheep wool in the building industry and in the removal of pollutants from the environment. *Processes* **2024**, *12*, 963. [CrossRef]
27. Picuno, P. Use of traditional material in farm buildings for a sustainablerural environment. *Int. J. Sustain. Built Environ.* **2016**, *5*, 451–460. [CrossRef]
28. Szatkowski, P.; Tadla, A.; Flis, Z.; Szatkowska, M.; Suchorowiec, K.; Molik, E. The potential application of sheep wool as a component of composites. *Rocz. Nauk. Pol. Towar. Zootech.* **2021**, *17*, 5. [CrossRef]
29. Giroud, J.P. Development of Criteria for Geotextile and Granular Filters. In Proceedings of the 9th Intternational Confonference on Geosynthetics, Guaruja, Brazil, 22–28 May 2010; Palmeira, E.M., Vidal, D.M., Sayao, A.S.J.F., Ehrlich, M., Eds.; International Geosynthetics Society: Jupiter, FL, USA, 2010; pp. 45–64.
30. Aydilek, A.H.; Oguz, S.H.; Edil, T.B. Constriction size of geotextile filters. *J. Geotech. Geoenvironmental Eng.* **2005**, *31*, 28–38. [CrossRef]
31. Rollin, A.L.; Lombard, G. Mechanisms affecting long-term filtration behavior of geotextiles. *Geotext. Geomembr.* **1988**, *7*, 119–145. [CrossRef]
32. Khan, M.W.; Dawson, A.R.; Marshall, A.M. A dynamic gradient ratio test apparatus. *Geotext. Geomembr.* **2018**, *46*, 782–789. [CrossRef]
33. Kalore, S.A.; Babu, G.L.S. Improved design criteria for nonwoven geotextile filters with internally stable and unstable soils. *Geotext. Geomembr.* **2022**, *50*, 1120–1134. [CrossRef]
34. Cazzuffi, D.; Ielo, D.; Mandaglio, M.C.; Moraci, N. Recent developments in the design of geotextile filters. In Proceedings of the 2nd International GSI—Asia Geosynthetics Conference, Seoul, Republic of Korea, 24–26 June 2015.
35. Rimoldi, P.; Shamrock, J.; Kawalec, J.; Touze, N. Sustainable use of geosynthetics in dykes. *Sustainability* **2021**, *13*, 4445. [CrossRef]
36. Broda, J.; Franitza, P.; Herrmann, U.; Helbig, R.; Große, A.; Grzybowska-Pietras, J.; Rom, M. Reclamation of abandoned open mines with innovative meandrically arranged geotextiles. *Geotext. Geomembr.* **2020**, *48*, 236–242. [CrossRef]
37. Wu, H.; Yao, C.; Li, C.; Miao, M.; Zhong, Y.; Lu, Y.; Liu, T. Review of Application and Innovation of Geotextiles in Geotechnical Engineering. *Materials* **2020**, *13*, 1774. [CrossRef] [PubMed]
38. Helbig, R.; Arnold, R.; Erth, H.; Roess, T.; Hevert, W.; Lischkowitz, H. New technologies for manufacturing extra coarse rope-like biodegradable geotextiles. *Tech. Textilien* **2006**, *49*, 185–187, 244–247.
39. Kaniuczak, J.; Stanek-Tarkowska, J.; Augustyn, Ł.; Szostek, M.; Knap, R.; Szewczyk, A. Wykorzystanie i ochrona zasobów powierzchni gruntów w województwie podkarpackim. *Inżynieria Ekol.* **2013**, *34*, 149–157. [CrossRef]
40. Grzybowska-Pietras, J.; Broda, J.; Przybyło, S.; Rom, M.; Laszczak, R.; Mitka, A. Zastosowanie innowacyjnych geotekstyliów z surowców odpadowych do zabezpieczenia gruntu przed erozją. *Inżynieria Morska Geotech.* **2015**, *4*, 615–620.
41. Sathishkumar, T.; Satheeshkumar, S.; Naveen, J. Glass fiber-reinforced polymer composites—A review. *J. Reinf. Plast. Compos.* **2014**, *33*, 1258–1275. [CrossRef]
42. Akil, H.M.; Omar, M.F.; Mazuki, A.A.M.; Safiee, S.; Ishak, Z.A.M.; Abu Bakar, A. Kenaf fiber reinforced composites: A review. *Mater. Des.* **2011**, *32*, 4107–4121. [CrossRef]
43. Faruk, O.; Bledzki, A.K.; Fink, H.P.; Sain, M. Biocomposites reinforced with natural fibers: 2000–2010. *Prog. Polym. Sci.* **2012**, *37*, 1552–1596. [CrossRef]
44. Staiger, M.P.; Tucker, N. 8—Natural-fibre composites in structural applications. Properties and Performance of Natural-Fibre Composites. In *Woodhead Publishing Series in Composites Science and Engineering*; Kim, L., Pickering, Eds.; Woodhead Publishing: Sawston, UK, 2008; pp. 269–300. [CrossRef]
45. Marczak, D.; Lejcuś, K.; Grzybowska-Pietras, J.; Biniaś, W.; Lejcuś, I.; Misiewicz, J. Biodegradation of sustainable nonwovens used in water absorbing geocomposites supporting plants vegetation. *Sustain. Mater. Technol.* **2020**, *26*, e00235. [CrossRef]
46. Grzybowska-Pietras, J.; Juzwa, A.; Nguyen, G. Wykorzystanie odpadowych włókien syntetycznych i wełny do zastosowań w inżynierii lądowej. *Przegląd Bud.* **2019**, *10*, 81–83.
47. Broda, J.; Gawłowski, A.; Grzybowska-Pietras, J.; Rom, M.; Przybyło, S.; Laszczak, R. Zastosowanie geotekstyliów do stabilizacji stromych skarp w kopalniach żwirowych. *Inżynieria Ekol.* **2017**, *18*, 71–77. [CrossRef]
48. Grzybowska-Pietras, J.; Nguyen, G.; Przybyło, S.; Rom, M.; Broda, J. Properties of meandrical geotextiles designed for the protection of soil against erosion. *E3S Web Conf.* **2018**, *49*, 00042. [CrossRef]
49. Nguyen, G.; Grzybowska-Pietras, J.; Broda, J. Application of innovative ropes from textile waste as an anti-erosion measure. *Materials* **2021**, *14*, 1179. [CrossRef]
50. Grzybowska-Pietras, J.; Juzwa, A. Biodegradowalne sznury Kemafil® w funkcji zabezpieczenia przeciwerozyjnego skarp. *GDMT Geoinżynieria Drog. Mosty Tunele* **2022**, *79*, 70–73.

51. Awal, A.S.M.A.; Mohammadhosseini, H. Green concrete production incorporating waste carpet fiber and palm oil fuel ash. *J. Clean. Prod.* **2016**, *137*, 157–166. [CrossRef]
52. Gyurkó, Z.; Jankus, B.; Fenyvesi, O.; Nemes, R. Sustainable applications for utilization the construction waste of aerated concrete. *J. Clean. Prod.* **2019**, *230*, 430–444. [CrossRef]
53. Alyousef, R.; Alabduljabbar, H.; Mohammadhosseini, H.; Mohamed, A.M.; Siddika, A.; Alrshoudi, F.; Alaskar, A. Utilization of sheep wool as potential fibrous materials in the production of concrete composites. *J. Build. Eng.* **2020**, *30*, 101216. [CrossRef]
54. Johnson, N.A.G.; Wood, E.J.; Ingham, P.E.; McNeil, S.J.; McFarlane, I.D. Wool as a technical fibre. *J. Text. Inst.* **2003**, *94*, 26–41. [CrossRef]
55. Daria, M.; Krzysztof, L.; Jakub, M. Characteristics of biodegradable textiles used in environmental engineering: A comprehensive review. *J. Clean. Prod.* **2020**, *268*, 122129. [CrossRef]
56. Cardamone, J. Biodeterioration of wool by microorganisms and insects. In *Bioactive Fibers and Polymers*; American Chemical Society: Washington, DC, USA, 2001; pp. 263–298. [CrossRef]
57. Queiroga, A.C.; Pintado, M.E.; Malcata, F.X. Potential use of wool-associated Bacillus species for biodegradation of keratinous materials. *Int. Biodeterior. Biodegrad.* **2012**, *70*, 60–65. [CrossRef]
58. Sun, Y.; Luo, J.; Ni, A.; Bi, Y.; Yu, W. Study on biodegradability of wool and PLA fibers in natural soil and aqueous medium. *Adv. Mater. Res.* **2013**, *641–642*, 82–86. [CrossRef]
59. Arshad, K.; Skrifvars, M.; Vivod, V.; Volmajer Valh, J.; Vončina, B. Biodegradation of Natural Textile Materials in Soil. *Tekstilec* **2014**, *57*, 118–132. [CrossRef]
60. Hutchinson, S.; Evans, D.; Corino, G.; Kattenbelt, J. An evaluation of the action of thioesterases on the surface of wool. *Enzym. Microb. Technol.* **2007**, *40*, 1794–1800. [CrossRef]
61. Chunhua, Z.; Liangjun, X.; Jiajing, Z.; Xin, L.; Weilin, X. Utilization of waste wool fibers for fabrication of wool powders and keratin: A review. *J. Leather Sci. Eng.* **2020**, *2*, 15. [CrossRef]
62. Broda, J.; Przybyło, S.; Kobiela-Mendrek, K.; Biniaś, D.; Rom, M.; Grzybowska-Pietras, J.; Laszczak, R. Biodegradation of sheep wool geotextiles. *Int. Biodeterior. Biodegrad.* **2016**, *115*, 31–38. [CrossRef]
63. Campanella, R.G.; Weemees, I. Development and use of an electrical resistivity cone for groundwater contamination studies. *Can. Geotech. J.* **1990**, *27*, 557–567. [CrossRef]
64. Davydov, V.A.; Baidikov, S.V.; Gorshkov, V.Y.; Malikov, A.V. Geophysics methods in electrometric assessment of dams. *Power Technol. Eng.* **2016**, *50*, 168–175. [CrossRef]
65. Michalis, P.; Sentenac, P. Subsurface condition assessment of critical dam infrastructure with non-invasive geophysical sensing. *Environ. Earth Sci.* **2021**, *80*, 556. [CrossRef]
66. Gruchot, A.; Zydroń, T.; Pařilková, J.; Zachoval, Z.; Cholewa, M.; Koś, K. Wykorzystanie spektrometrii impedancyjnej do monitorowania przepływu filtracyjnego przez nasypy hydrotechniczne. *Acta Sci. Pol. Archit.* **2018**, *17*, 55–65. [CrossRef]
67. Drahor, M.G.; Göktürkler, G.; Berge, M.A.; Kurtulmuş, T.Ö. Application of electrical resistivity tomography technique for investigation of landslides: A case from Turkey. *Environ. Geol.* **2006**, *50*, 147–155. [CrossRef]
68. *PKN-CEN ISO/TS 17892-4:2009*; Badania Geotechniczne. Badania Laboratoryjne Gruntów. Część 4: Oznaczanie Składu Granulometrycznego. Polski Komitet Normalizacyjny: Warszawa, Poland, 2009.
69. *PKN-CEN ISO-TS 17892-11:2009*; Badania Geotechniczne. Badania Laboratoryjne Gruntów. Część 11: Badanie Filtracji Przy Stałym i Zmiennym Gradiencie Hydraulicznym. Polski Komitet Normalizacyjny: Warszawa, Poland, 2009.
70. *PN-EN ISO 14688-2:2006/Ap2*; Badania Geotechniczne. Oznaczanie i Klasyfikowanie Gruntów. Cześć 2: Zasady Klasyfikowania. Polski Komitet Normalizacyjny: Warszawa, Poland, 2006.
71. Tabbagh, A.; Dabas, M.; Hesse, A.; Panissod, C. Soil resistivity: A non-invasive tool to map soil structure horizonation. *Geoderma* **2000**, *97*, 393–404. [CrossRef]
72. de Jong, S.M.; Heijenk, R.A.; Nijland, W.; van der Meijde, M. Monitoring soil moisture dynamics using electrical resistivity tomography under homogeneous field conditions. *Sensors* **2020**, *20*, 5313. [CrossRef]
73. Woźniak, T.; Bania, G.; Mościcki, W.J.; Ćwiklik, M. Electrical resistivity tomography (ERT) and sedimentological analysis applied to investigation of Upper Jurassic limestones from the Krzeszowice Graben (Kraków Upland, southern Poland). *Geol. Q.* **2018**, *62*, 287–302. [CrossRef]
74. Mościcki, W.J.; Bania, G.; Ćwiklik, M.; Borecka, A. DC resistivity studies of shallow geology in the vicinity of Vistula River flood bank in Czernichów village (near Kraków in Poland). *Stud. Geotech. Mech.* **2014**, *36*, 63–70. [CrossRef]
75. Bougoul, S.; Ruy, S.; de Groot, F.; Boulard, T. Hydraulic and physical properties of stonewool substrates in horticulture. *Sci. Hortic.* **2005**, *104*, 391–405. [CrossRef]
76. Kołodziej, B.; Bryk, M.; Otremba, K. Effect of rockwool and lignite dust on physical state of rehabilitated post-mining soil. *Soil Tillage Res.* **2020**, *199*, 104603. [CrossRef]
77. Van Genuchten, M.T. A closed-form equation for predicting the hydraulic conductivity of unsaturated soils. *Soil Sci. Soc. Am. J.* **1980**, *44*, 892–898. [CrossRef]
78. Cannavo, P.; Hafdhi, H.; Michel, J.-C. Impact of Root Growth on the Physical Properties of Peat Substrate under a Constant Water Regimen. *Hortscience* **2011**, *46*, 1394–1399. [CrossRef]
79. Bisong, E. Google Colaboratory. In *Building Machine Learning and Deep Learning Models on Google Cloud Platform*; Apress: Berkeley, CA, USA, 2019. [CrossRef]

80. Harris, C.R.; Millman, K.J.; van der Walt, S.J.; Gommers, R.; Virtanen, P.; Cournapeau, D.; Wieser, E.; Taylor, J.; Berg, S.; Smith, N.J.; et al. Array programming with NumPy. *Nature* **2020**, *585*, 357–362. [CrossRef]
81. Reback, J.; McKinney, W.; Van den Bossche, J.; Augspurger, T.; Cloud, P.; Klein, A.; Roeschke, M.; Tratner, J.; She, C.; Ayd, W.; et al. *Pandas-Dev/Pandas, Pandas 1.0.0*; Zenodo: Geneva, Switzerland, 2020. [CrossRef]
82. Hunter, J.D. Matplotlib: A 2D Graphics Environment. *Comput. Sci. Eng.* **2007**, *9*, 90–95. [CrossRef]
83. Waskom, M.L. Seaborn: Statistical data visualization. *J. Open Source Softw.* **2021**, *6*, 3021. [CrossRef]
84. *PN-EN ISO 14688-2:2018-05*; Rozpoznanie i Badania Geotechniczne. Oznaczanie i Klasyfikowanie Gruntów. Część 2: Zasady Klasyfikowania. Polski Komitet Normalizacyjny: Warszawa, Poland, 2018.
85. Judycki, J.; Jaskuła, P.; Pszczoła, M.; Alenowicz, J.; Dołżycki, B.; Jaczewski, M.; Ryś, D.; Stienss, M. *Katalog Typowych Konstrukcji Nawierzchni Podatnych I Półsztywnych*; Politechnika Gdańska: Gdańsk, Poland, 2013.
86. Website of the Institute of Meteorology and Water Management, National Research Institute. Available online: https://danepubliczne.imgw.pl/ (accessed on 20 July 2023).